The effect of the yield to tensile strength ratio on the stress field in stress/strain concentrations around holes in steel structures

S.F.P.M. Obers

TU Delft

The effect of the yield to tensile strength ratio on the stress field in stress/strain concentrations around holes in steel structures

by

S.F.P.M. Obers

to obtain the degree of Master of Science
at the Delft University of Technology,

Student number:	4373677
Project duration:	November 16, 2020 - July 30, 2021
Dr. C.L. Walters,	TU Delft, supervisor
W.J. Wong,	TU Delft
Dr. X. Jiang,	TU Delft
Ir. J.J. Overal,	Huisman Equipment, daily supervisor
Ir. E. Romeijn,	Huisman Equipment, supervisor

TU Delft Delft University of Technology

Huisman
Equipped for impact

Abstract

The aim of this thesis is to determine the influence of the Y/T, yield to tensile strength, ratio on the stress fields of high strength steels. This is relevant to the offshore industry as regulations restrict the use of steels with a high yield to tensile strength ratio, which is a characteristic of high-strength and ultra high-strength steels. Identifying the influence of these parameters on behavior could lead to a scientific underpinning and review of the rules. The focus of this thesis is on stress concentrations at circular cutouts under uniform tension. The local stress and strain was found, which could be used to assess the risk of strain localization and fracture.

Analytical models of Stowell, Neuber and Irwin are used to establish new relationships between the Y/T ratio and the stress field. The analytical methods of Stowell and Neuber were able to account for strain hardening, while the Irwin analytical relationship only provides a elastic-perfectly plastic solution. Besides the stress field, an analytical formulation for the local strain based on Stowell's theory is also established.

Numerical simulations were carried out for S690, S960, and S1100 materials. The numerical material models are later used in the research to validate analytical approaches. Also, an infinite plate approach is applied to the specimens by scaling the ligaments of the specimens by a factor of 6.

A parametric study has been carried out to gain insights into the influence of the governing parameters in relation to local strain. The parameters studied are the Y/T, yield strength, strain hardening exponent, and strength coefficient. Each parameter is varied separately.

The main conclusions are that a high Y/T ratio causes a slight decrease in plastic stress concentration factor, resulting in a slight increase in local strain. The strain hardening exponent shows the same trend, but the changes are even less significant. The yield strength and strength coefficient have no effect on the stress concentration factor or local strain. None of the parameters show any influence on the extent of the plastic zone of the material.

Preface

This study was proposed by a combination of Huisman Equipment and the TU Delft. The study is part of a Joint Industry Project called “HYSt: High Y/T Steel”, whose main objective is to safely expand the application of high strength structural steels with a nominal yield strength of 690 MPa or more.

This study is carried out as Master Thesis Project at the Section Ship and Offshore Structures, Faculty 3mE, Delft University of Technology. In general, I would like to thank Huisman Equipment and the Section of Ship and Offshore Structures of the Delft University of Technology for making this study possible. I would like to express my appreciation to my daily supervisor at Huisman Equipment, Jaap Overal, and my weekly supervisor Eric Romeijn. I would also like to thank my daily supervisor at the University of Technology, Dr. C. L. Walters, for his efforts.

Lastly, I would like to thank my girlfriend for all her support along the way. My family and friends, for the distractions and support. And my roommates for reminding me to use free time as social time instead of study time.

S.F.P.M. Obers
Delft, July 2021

Contents

Nomenclature

δ	Change in gauge length in mm
ϵ	Dimensionless strain
ϵ_y	Dimensionless yield strain
σ	Stress in N/mm^2
σ_0	Flow stress in N/mm^2
σ_θ	Tangential stress in N/mm^2
σ_I, σ_{II}, σ_{III}	Principal stress in N/mm^2
σ_r	Radial stress in N/mm^2
$\sigma_{0.2}$	Stress at 0.2 yield offset in N/mm^2
σ_{eq}	Equivalent stress in N/mm^2
σ_{ff}	Far-field stress in N/mm^2
σ_{max}	Nominal stress in N/mm^2
σ_{True}	True stress in N/mm^2
σ_{xx},σ_{yy}	Normal stress in respectively x and y direction in N/mm^2
$\tau_{r\theta}$	Shear stress in N/mm^2
θ	Angle in rad
A_0	Initial cross-section in mm^2
a_0	Original thickness of specimen in mm
a_{eff}	Effective crack length in mm
b_0	Original width of parallel length of specimen in mm
E	Elasticity modulus in N/mm^2
E_∞	Secant modulus of elasticity far from hole in N/mm^2
E_S	Secant modulus of elasticity at maximum stress in N/mm^2
f_y	Yield stress in N/mm^2
FEA	Finite Element Analysis
K	Strength coefficient in N/mm^2
k	Dimensionless gauge length constant
K_I	Dimensionless stress intensity factor for mode I
K_{eff}	Dimensionless effective stress intensity factor
L_0	Initial gauge length in mm

L_c	Parallel length of specimen in mm
L_t	Total length of specimen in mm
n	Dimensionless hardening parameter
P	Applied load in N
S	Applied loading in N
S_0	Initial cross-sectional area of parallel length in mm^2
SCF	Dimensionless Stress Concentration Factor
Y/T	Dimensionless yield strenght to tensile strength ratio

1 Introduction

Over the years, new, higher strengths of steel have found their way into the construction and manufacturing industries. These higher strengths of steel are more attractive to manufacturers and builders because they are stronger (i.e., have a higher yield strength). This has the advantage of requiring less material to achieve the same result: a safely designed structure with a lower structural weight. The aforementioned advantage is a particularly relevant development for cranes on floating vessels because cranes are structures located high above the keel, where mass reduction leads to increased stability and increased capacity. In addition, the effects of weight reduction can have a positive impact on costs, even if the material is more expensive. Therefore, the introduction of higher strengths of steel could make a promising contribution to the crane construction industry.

Higher strength steels introduce challenges in terms of design rules set by certification companies. These set limits on the yield strength to tensile strength ratio to ensure structural safety [5, 7–9, 19–21, 27, 32, 33, 39, 40]. These limits are based on nominal values or actual values obtained from standard tensile tests [42]. The reason for introducing these rules is to ensure a sufficiently high margin of safety before the material fails and dangerous situations arise. This is a problem for higher strengths of steel, where the yield strength is closer to the tensile strength than for lower strengths of steel and therefore the allowable limits are exceeded. Higher strengths of steel may then not be fully utilized in terms of weight and consequently cost. There is a need for research to capture the behavior of these types of steel and ultimately to extend their application by revising the design rules. The global objective is to find the influence of the yield to tensile strength ratio on the failure load of high strength steels. This research will partially address this objective. The main objective of this research is to determine the influence of the yield strength to tensile strength ratio on the stress field of high strength steels induced by a discontinuity in order to evaluate the effects on the material behavior. Specimens with a discontinuity experience stress concentrations that result in large local strains. These local strains are the governing factor for ductile failure and therefore important to evaluate. The research question is formulated as follows:

What is the influence of the yield strength to tensile strength ratio on the stress fields of high strength steels?

The aim of this study is to answer the research question. Therefore, the following sub-questions are introduced which will help in answering the main question.

- How can a stress field around a stress concentration be described analytically?
- What is the best way to describe the strain hardening behavior of high strength steels?

1.1. Report Structure

To answer the sub-questions and ultimately the research question, this thesis begins with a literature review in Chapter 2, followed by a discussion of the methodology and scope in Chapter 3. Chapter 4 describes analytical models that can approximate the behavior of high strength steels under uniform tension. Numerical FEA models are discussed in Chapter 5. After that, the numerical FEA models are calibrated in Ansys software to simulate the behavior of high strength steels with a stress concentration in Chapter 6. Also, the analytical models will be validated in this chapter. Then, the results of the numerical simulations and analytical formulas are presented in Chapter 7, including an analysis of the findings. A conclusion is then drawn in Chapter 8. Finally, a discussion and recommendation for future research is written in Chapter 9. Appendix A contains the experimental results of the standard tensile tests of Stofregen and VTT. Appendix B contains design cases relevant for Huisman Equipment.

2

Literature Review

The literature review marks the beginning of the research project on the relationship between yield strength over tensile strength with the stress field. The topics presented below are interrelated and should be relevant to achieve the end goal of answering the research question. The main focus of the literature review is on high strength steel plates in tension. Further specification of the scope can be found in Chapter 3.

2.1. Theoretical background

To achieve a general understanding of the topics discussed in the remaining sections, a description of stress-strain behavior of steel is provided in this section. All topics discussed in this section will be used later in the applied theories or proposed experimental data.

2.1.1. Standard tensile test

To describe the behavior of materials after tension has been applied, stress and strain are essential parameters. Equation (2.1) can be used to determine the nominal stress in materials, also known as the engineering stress. Here, P is the applied load in N, A_0 is the original net cross-section in mm^2, and σ is the stress in N/mm^2 [11].

$$\sigma = \frac{P}{A_0} \tag{2.1}$$

Similarly, the nominal strain, also known as engineering strain, can be calculated using Equation (2.2). Here, L_0 is the original gauge length in mm and δ is the change in gauge length in mm .

$$\epsilon = \frac{\delta}{L_0} \tag{2.2}$$

To show the relationship between the engineering stress and the engineering strain of a particular specimen, a stress-strain curve is constructed with a standard tensile test such as the International Organization of Standardization (ISO) [24]. In this test, a specimen is clamped on one side, and monotonic tension is applied on the other side. The applied tension is increased, and the analogous change in gauge length is followed until failure. A schematic specimen with the specified variables is shown in Figure 2.1. Here, a_0 is the original thickness, L_0 is the original gauge length, and S_0 is the original cross-sectional area of the parallel length. An example of the stress-strain curve is shown in Figure 2.2. In this graph, the x-axis is described by strain and the y-axis by stress. A standard tensile test can be used to calculate the relationship between yield strength and tensile strength (Y/T).

If the actual values of the cross-sectional area are used and the length of the specimen at the time of loading is measured, then it is referred to as true stress and true strain. This is shown in Figure 2.2 for S355 steel, and given in Equations (2.3) and (2.4).

$$\sigma_{true} = \sigma_{engineering} \cdot (1 + \epsilon_{engineering}) \tag{2.3}$$

$$\epsilon_{true} = ln(1 + \epsilon_{engineering}) \tag{2.4}$$

Figure 2.2 also shows the elastic region, yielding region, strain hardening region, and the region where necking occurs. The necking consists of a considerable amount of localization of strain. When necking occurs, conversion from engineering stress/strain value to true stress/strain values is not valid as the assumption $L \cdot A = L_0 \cdot A_0$ does not hold anymore. The other areas mentioned are briefly discussed in the following subsections. In addition, the yield stress and the ultimate stress are given. In the elastic region, Hooke's law, shown in Equation (2.5), is applied. Figure 2.2 also shows the engineering stress-strain curves resulting from a standard tensile test for S1100, S690 and S355 steel.

$$\sigma = E \cdot \epsilon \tag{2.5}$$

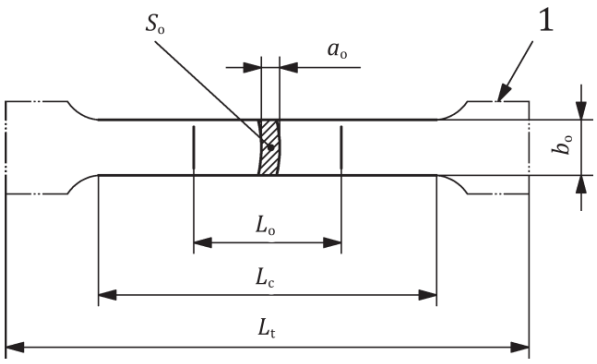

Figure 2.1: EN ISO 6892-1 Configuration test piece [24]

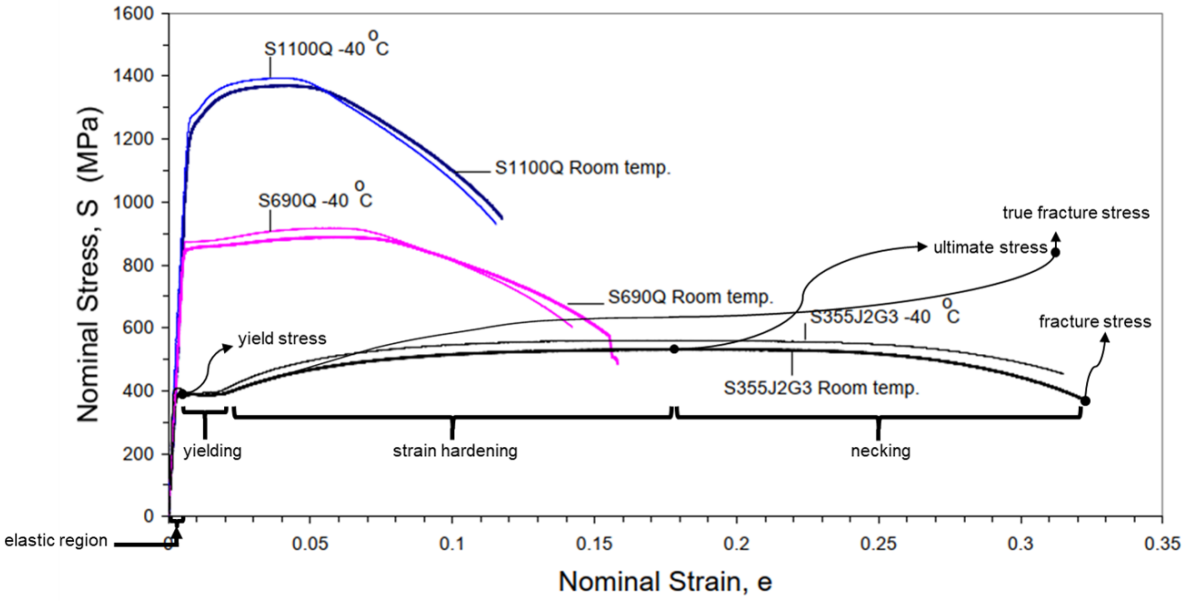

Figure 2.2: Engineering stress-strain curve for ductile S1100, S690 , and S355 steel at room temperature and -40 °C [35]

Saint-Venant principle

In a standard tensile test to determine the stress-strain behavior, the boundary conditions may have an effect on the behavior of the stress. The Saint-Venant principle states that if a load on a plate or bar, that causes deformation on the support and on the applied load, is far enough away from the support,

a uniform stress is obtained between the applied load and the support [11]. This principle is of great importance when studying the behavior of stress concentrations in a standard tensile test. In the best case, the stress concentration is not affected by the applied load, so that a purely discontinuity- induced stress concentration can be studied.

2.1.2. Yield criterion

Isotropic yielding of the material is often described by the von Mises yield criterion. The von Mises yield criterion is described by equation (2.6), where all three principal stresses are involved [43]. The von Mises criterion gives the critical value of elastic stress in a material.

$$\sigma_0 = 2^{-1/2}\left[(\sigma_{\mathrm{I}} - \sigma_{\mathrm{II}})^2 + (\sigma_{\mathrm{II}} - \sigma_{\mathrm{III}})^2 + (\sigma_{\mathrm{III}} - \sigma_{\mathrm{I}})^2\right]^{1/2} \tag{2.6}$$

2.1.3. Stress concentration

When discontinuities exist in the material with an applied load, stress concentrations occur. To represent these stress concentrations, a stress concentration factor K_t is introduced. This factor gives the ratio between the maximum stress and the mean normal stress applied to the cross section [11]. The stress concentration factor K_t is described mathematically by equation 2.7.

$$K_t = \frac{\sigma_{max}}{\sigma_{avg}} \tag{2.7}$$

Causes of stress concentrations are holes, corners, cut-outs, notches and welded joints which can have a significant impact on structural integrity, as local yielding of the material occurs at the locations of stress concentrations.

2.1.4. Describing stress-strain behavior

Figure 2.2 shows the stress-strain relationship as a result of a standard tensile test on a ductile material. In this figure, an elastic region is shown where stress and strain have a linear relationship. At higher strains, yielding occurs and the material starts to behave plastically and thus nonlinearly. For modelling purposes, this behavior can be approximated using various approaches [44] [31]:

- Elastic
- Elastic, perfectly plastic, see figure 2.3
- Elastic, nonlinear hardening model, see figure 2.4

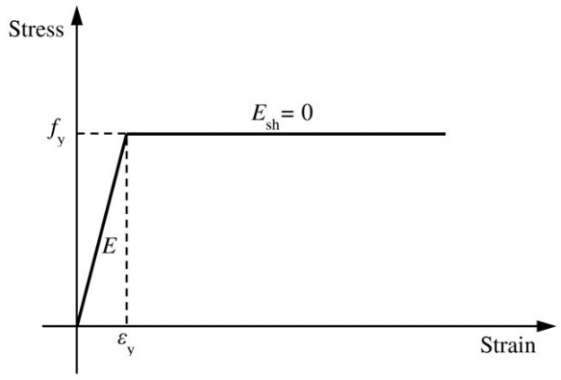

Figure 2.3: Elastic-perfectly plastic behavior of the engineering stress-strain relationship [44]

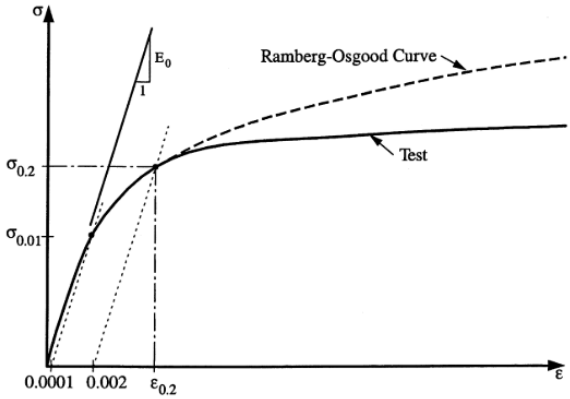

Figure 2.4: Elastic non-linear behavior of the engineering stress-strain relationship of austenitic UNS30400 (AISI304) stainless steel [31]

Hardening

As shown in Figure 2.2, the stress-strain curve shows an increase in stress in the plastic region. This increase is caused by hardening. Hardening, or strain hardening, is a process in which the yield point of a steel specimen increases due to plastic straining. Hardening is achieved by loading the material beyond the yield point where after the load is removed, the yield point is increased [11]. The

yield strength is then increased. For this research, isotropic hardening is considered assuming the yield plane to extend in all directions.

2.1.5. High strength steel versus lower strength

As briefly indicated in the introduction, the yield strength of higher strength steels is closer to the tensile strength than milder steel. This ultimately leads to challenges in terms of design rules that require a specific Y/T limit [5, 7–9, 19–21, 27, 32, 33, 39, 40]. Figure 2.2 graphically shows the main difference between high strength steel S355, and extra high strength steels S690 and S1100. As indicated, the yield stress of the high strength steel is higher compared to the lower strength steels. The ultimate tensile strength does not follow the same trend. As a result, the Y/T ratio is higher.

2.1.6. Necking

To determine the strain corresponding to the onset of necking (at ultimate tensile strength) in the stress-strain curve, obtained with the standard tensile test, the Considère condition can be used [4]. This condition uses the history of the stress-strain behavior and states that the derivative of the equation given in (2.8) is equal to zero at the point of necking. Here, F is the applied force in N, σ is the stress in N/mm^2, and A is the cross section in mm^2.

$$F = \sigma \cdot A \tag{2.8}$$

Provided that the strain increment is equal to equation (2.9), the final relationship can be found, which is shown in equation (2.10).

$$\partial\epsilon = -\frac{\partial A}{A} \tag{2.9}$$

$$\sigma = \frac{\partial\sigma}{\partial\epsilon} \tag{2.10}$$

2.1.7. Ductile fracture

As described in Subsection 2.1.1, failure by excessive plastic deformation is the governing failure mechanism. This mechanism is associated with ductile fracture. A high material toughness combined with a relatively high material temperature results in ductile behavior, as opposed to, brittle behavior.
Ductility is necessary to provide an energy distribution that prevents local failure. Global yielding should be achieved before local fracture occurs, otherwise the load bearing capacity of the material is not utilised [34]. Therefore, ductility is an important property for structures with high peak loads, such as steel cranes. The yield to tensile strength ratio, Y/T ratio, can be related to the ductility of the material [34]. A ratio close to 1 indicates a low hardening capacity, and a ratio closer to zero indicates in a higher hardening capacity. This results, respectively, in low and high material ductility. Strain hardening behavior is further discussed in subsection 2.1.4. In this research, high strength steels with ductile behavior and therefore ductile fracture are considered.

2.2. Models describing stress concentration factor

In this section, an available model for describing stress concentration factors of materials under tensile loading is discussed in more detail.

The study by Stowell in 1950 [36] based on Kirsch's study in 1898 [14], describes the stress concentration around a circular cutout in a plate under uniform tension. In the study of Stowell, a perfectly elastic, infinitely long, isotropic and in-compressible material is assumed. A sketch of the plate with circular cutout under uniform tension S, equal to the nominal stress σ_{nom} is shown in Figure 2.5. The nominal stress is calculated with a net cross section of a specimen without taking into account a discontinuity. Due to the assumption of an infinitely large plate, the Saint-Venant principle can be applied, which is discussed in Section 2.1.
Equations (2.11) to (2.13) analytically describe the elastic-plastic stress concentration factor. Here, σ_r is the radial stress, σ_θ is the tangential stress, $\tau_{r\theta}$ is the shear stress and σ_{nom} is the nominal stress.

$$\frac{\sigma_r}{\sigma_{nom}} = \frac{1}{2}\left(1 - \frac{a^2}{r^2}\right) + \frac{1}{2}\left(1 + \frac{3a^4}{r^4} - \frac{4a^2}{r^2}\right)\cos 2\theta \tag{2.11}$$

$$\frac{\sigma_\theta}{\sigma_{nom}} = \frac{1}{2}\left(1 + \frac{a^2}{r^2}\right) - \frac{1}{2}\left(1 + \frac{3a^4}{r^4}\right)\cos 2\theta \tag{2.12}$$

$$\frac{\tau_{r\theta}}{\sigma_{nom}} = -\frac{1}{2}\left(1 - \frac{3a^4}{r^4} + \frac{2a^2}{r^2}\right)\sin 2\theta \tag{2.13}$$

Except from the elastic solution Stowell also presents a solution for the SCF which is also accounts for yielding of the material in Equations (2.14) to (2.16). Here, E_s is the secant modulus at the point (r, θ) and $E_{s,\infty}$ is the secant modulus at $r = \infty$.

$$\frac{\sigma_r}{\sigma_{nom}} = \frac{1}{2}\left(1 - \frac{a^2}{r^2}\right) + \frac{E_s}{E_{s,\infty}} \cdot \frac{1}{2}\left(1 + \frac{3a^4}{r^4} - \frac{4a^2}{r^2}\right)\cos 2\theta \tag{2.14}$$

$$\frac{\sigma_\theta}{\sigma_{nom}} = \frac{1}{2}\left(1 + \frac{a^2}{r^2}\right) - \frac{E_s}{E_{s,\infty}} \cdot \frac{1}{2}\left(1 + \frac{3a^4}{r^4}\right)\cos 2\theta \tag{2.15}$$

$$\frac{\tau_{r\theta}}{\sigma_{nom}} = -\frac{1}{2} \cdot \frac{E_s}{E_{s,\infty}} \cdot \left(1 - \frac{3a^4}{r^4} + \frac{2a^2}{r^2}\right)\sin 2\theta \tag{2.16}$$

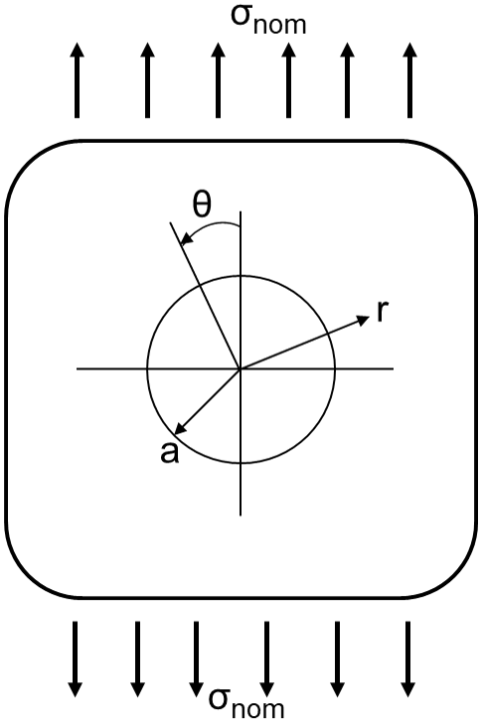

Figure 2.5: Plate with circular cutout with applied uniform tension

2.3. Models describing hardening behavior

The non-linear hardening behavior of high strength steels can be described by power laws and other types. These formulations are all based on an empirical approach, since they are used to approximate as closely as possible the stress-strain behavior based on an existing stress-strain curve. This section, briefly describes the most common hardening laws in the literature and shows relationships between the hardening parameter and the Y/T ratio that are analytically and empirically based.

Much work has been done to approximate the stress-strain behavior by providing the best possible description of hardening. Models exist in the literature such as Hollomon's power law [16], Swift-Voce

[37], the Ramberg-Osgood relationship [10], various variations of the Ramberg-Osgood relationship [10, 30, 31], a quad-linear stress-strain model [44] and a bilinear plus nonlinear hardening model [44]. The power-type hardening laws are extensions of the pure power law for hardening. This basic form is shown in equation (2.17). Here σ is the stress in N/mm^2, ϵ is the dimensionless strain, n is the strain hardening exponent, and K is the strength coefficient. The fitting parameters K and n can be determined using a standard tensile test.

$$\sigma = K\varepsilon^n \tag{2.17}$$

Research by Bannister and Leis shows that the hardening exponent n can be related to the Y/T ratio [3, 17]. This may be relevant to the relationship between the stress concentration factor and the Y/T ratio if the stress concentration factor can be related to the hardening exponent via a hardening law.

Bannister investigated the influence of the Y/T ratio in 1999 and established a conservative relationship between the Y/T ratio and the hardening exponent n [3]. The relationship is shown in Equation (2.18).

$$\mathrm{n} = 0.3(1 - \frac{Y}{T}) \tag{2.18}$$

A study by Leis on the failure assessment of corroded pipelines showed an analytical relationship between the Y/T ratio and the hardening exponent [17]. This relationship is given in Equation (2.19). Here, ϵ_y' is the yield strain and, e is Euler's number.

$$\frac{Y}{T} = \frac{1}{1+\varepsilon_y}\left[\frac{e \cdot \ln\left(1+\varepsilon_y\right)}{n}\right]^n \tag{2.19}$$

2.4. Elastic-plastic analysis models at discontinuities

Stress concentrations and hence peak stresses are induced by geometric discontinuities in materials subjected to a certain loading. Locally, these peak stresses can be several times the yield strength, causing local plastic deformations [15][38]. Since the peak stresses can be high above the yield stress, a distorted picture of reality is shown, and structures could end up being designed too conservatively. Therefore, methods are developed to calculate the elastic-plastic stress and strain at a notch. Stowells and Neubers method can be used to calculate this stress and strain [28].

2.4.1. Stowell

To calculate elasto-plastic stresses and strains at a notch the equations from the study from Kirsch in 1898 are rewritten by Stowell. These equations account for the plastic behavior of the material which results in the radial stress, tangential stress and shear stress shown in Equations (2.14) to (2.16) and discussed in Section 2.2.

2.4.2. Neuber

In 1961, Neuber's method was developed in for monotonic shear stress on prismatic bodies. But, according to Neuber, it can "Be generalized for arbitrary loading states in notches by means of one of the well-known theories of failure" [25]. The value of the theoretical stress concentration factor K_t is equal to the square root of the stress and strain concentration factors, i.e. the geometric mean value according to Neuber [26]. Hooke's law combined with the geometric mean, and the Ramberg-Osgood equation are shown in Equations (2.5), (2.20), and (2.21). These equations can be used to determine the relationship shown in Equation (2.22) [15].

$$\varepsilon = \frac{\sigma}{E} + \left(\frac{\sigma}{H}\right)^{1/n} \tag{2.20}$$

$$K_t^2 \cdot \sigma_{nom} \cdot \epsilon_{nom} = \sigma \cdot \epsilon \tag{2.21}$$

$$\frac{\left(\sigma_{\mathrm{nom}} k_t\right)^2}{E} = \frac{\sigma^2}{E} + \sigma\left(\frac{\sigma}{H}\right)^{1/n} \tag{2.22}$$

Here, σ_{nom} is the nominal stress in N/mm^2, k_t the stress concentration factor, E the elasticity

modulus in N/mm^2, σ the actual stress in N/mm^2, ϵ is the actual dimensionless strain, H the strength coefficient in N/mm^2 and n is the hardening exponent. The nominal stress is the applied load divided by the net cross-sectional area. The Ramberg-Osgood relation is used for the relationship between stress and corresponding strain. Neuber's method assumes that the strain energy density of a pseudo-elastic problem is equal to the strain energy density of the actual elasto-plastic problem [15]. This assumption is visually represented in Figure 2.6. It also assumed that Equation (2.22) holds for a plate in tension as originally derived for shear strained notches in prismatic bodies [26]. Elastic-plastic behavior at the notch root and elastic behavior at the nominal cross-section are also assumed.

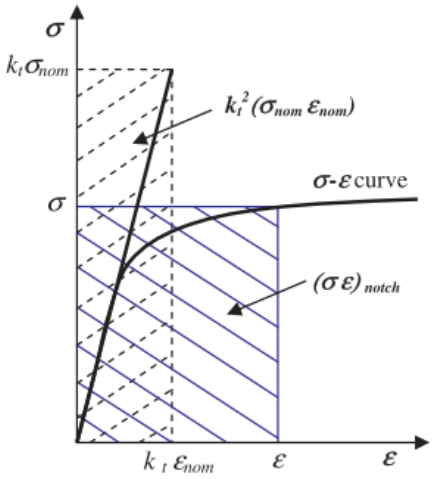

Figure 2.6: Energy redistribution Neuber [15]

2.4.3. Applicability of Neubers and Stowells method

These equations established by Stowell and Neuber can be used to describe the behavior at a notch root or at a circular cutout. These equations can also be used for redistribution of energy in the elastic zone to the elastic-plastic zone. A disadvantage of these methods is the assumption that the "total strain energy density of pseudo-elastic problem is equal to the total strain energy density of actual elasto-plastic problem"[15]. Moreover, isotropic behavior, incompressibility and an infinite plate are assumed.

2.4.4. Dugdale and Irwin model

The Dugdale and Irwin model come from the field of fracture mechanics. The Dugdale model describes the plastic zone around a crack. This model relates the amount of plastic yielding to the applied load [6]. The Dugdale model is based on an ideal elastic-plastic material of a plate with infinite length. This model evaluates plastic deformation in a line parallel to the crack-tip, which does not results in a realistic representation of plastic behavior at stress concentrations without cracks because plasticity around stress concentrations is not formed in a line [13].

Another method for crack-tip yielding is the Irwin approach [1]. This approach assumes that the boundary between elastic and plastic occurs when equation (2.23) satisfies the set yield condition set. σ_{yy} is then equal to the yield stress. In the given equation, σ_{xx} is the stress in x-direction in N/mm^2, σ_{yy} is the stress in y-direction in N/mm^2. K_I is the dimensionless stress intensity factor, r is the radius in polar coordinates. The yield stress is implemented for σ_{yy} and the equation is solved for r. Then the same approach is implemented as in the Neuber, ESED and Hardrath and Ohman methods, a force equilibrium between the elastic and plastic zonse is applied, graphically shown in Figure 2.7. By defining an effective crack length, the softening of the material in the plastic zones is taken into account. To account for this, an iterative solution is required, as no plasticity correction was previously implemented. Equation (2.24) describes the form of the effective stress intensity that must be iterated. The approach by Irwin could also be promising for a stress concentration factor instead of a stress intensity factor, since a plastic correction due to softening of the material is accounted for.

$$\sigma_{xx} = \sigma_{yy} = \frac{K_I}{\sqrt{2 \cdot \pi \cdot r}} \tag{2.23}$$

$$K_{eff} = Y\left(a_{eff}\right)\sigma\sqrt{\pi a_{eff}} \tag{2.24}$$

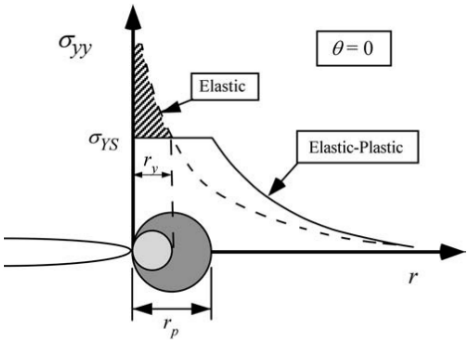

Figure 2.7: Graphical representation of the force equilibrium by Irwin [1]

Irwin's approach is a description of the plastic zone for a crack, but this method can be used as an analogy for application on a stress concentration factor. It is advantageous to correct for the plastic zone. Irwin's method does not account for strain hardening and therefore assumes perfect plasticity.

2.5. Available test results

The aim of the research is to find the influence of the Y/T ratio on the stress field for high strength steels under tension. This objective could be achieved by finding a general relationship between Y/T and a stress concentration in an analytical way. This analytical solution should be validated via Finite Element Analysis (FEA). Therefore, the FEA should be validated with experimental results from standard tensile tests.
Test data from Stofregen [35] and VTT is available to validate the FEA models [12]. Where Stofregen tested double sided notched (2 and 4 mm radius) extra high strength steel specimens (S690 and S1100) and VTT tested extra high strength steels (S960) with a circular cutout of different sizes. All tests were carried out in accordance with ISO6892-1 [24].

2.5.1. Test data from M. Stofregen

Stofregen's tensile test data is shown in Figures A.1 to A.3 in Appendix A [35]. Important parameters associated with these tests are given in table 2.1. The orientation of the material is in the rolling direction (longitudinal direction) of the steel which is the same for all specimens and the material is assumed being isotropic. The layout of the specimen will be further discussed in Section 5.1.

Table 2.1: Overview important parameters S690 and S1100 standard tensile test

Material grade	S690+S1100	$[MPa]$
Cross section S_0	300	$[mm^2]$
Gauge length L_0	97.8	$[mm]$
Applicable code	EN 6892-1	$[-]$
Repetitions	2	$[-]$

2.5.2. Test data from VTT

The standard tensile tests performed by VTT provide information on the stress-strain behavior of a specimen with a central circular hole of varying dimensions. The data is given in Figure A.4 in Appendix A. This data are converted from a force-displacement curve to a stress-strain curve, with a correction for the reduced initial cross-section due to the hole. Important parameters associated with these tests are given in Table 2.2.

Table 2.2: Overview important parameters S960 standard tensile test

Material grade	S960	$[MPa]$
Cross section S_0	640	$[mm^2]$
Gauge length L_0	142.93	$[mm]$
Applicable code	EN 6892-1	$[-]$
Repetitions	2	$[-]$

2.6. Conclusion

In the literature study, the influence of the yield to tensile strength ratio on the stress field of high strength steels is investigated. It is divided into models describing the stress concentration factor, models describing hardening behavior, elastic-plastic analysis of notches, and available test results.

Models describing stress fields can be divided into two categories: analytical models and empirical models. Analytical models are useful because they are generally applicable. The state of the art for analytical formulations is described by Stowell [36]. For empirical models, the most recent published work is by Deborah, Zhuming and Pilkey [29].

Regarding hardening behavior of high strength steels, relevant models such as Hollomon's power law and Ramberg-Osgood can be applied. The pure power hardening law is the simplest and thus most easily applicable form of describing the hardening behavior. Therefore, it is most suitable for further research using this model.

The most useful approaches for this study of material behavior at discontinuities is described by Neuber, Stowell and Irwin [1, 18, 23, 36]. A distinction can be made in the relationship between elasticity and plasticity, where Neuber and Stowell assume energy equality and Irwin corrects for softening due to plasticity. Also, relationships are found by Leis between the hardening exponent n and the Y/T ratio, which are useful in determining the influence of the Y/T ratio on stress concentrations [17].

Test data of high strength steels, S690 to S1100, are found in literature. These steels are tested with notches and cutouts by Stofregen [35] and VTT [12]. The results can be used for validation purposes to check the relationship between Y/T and the stress concentration factor at the end.

2.6.1. Research gap

After drawing conclusions regarding the literature related to the main research question, a research gap is identified. To answer the research question, a model should be available that relates the Y/T ratio to a stress field in the vicinity of a discontinuity of high strength steel. Several aspects of this model are found in the literature, such as analytical/empirical formulations of the stress concentration factor of structures with a discontinuity. Models describing the hardening behavior of the material are also found. Furthermore, relationships between the hardening exponent and the Y/T ratio are found. Test results of high strength steels with discontinuities are also found. But, a relationship between the Y/T ratio and stress fields for high strength steels is not found in literature. This defines the research gap. The methodology used to fill this research gap is discussed in Chapter 3.

3

Methodology and scope

The aim of this report is to answer the main question by formulating an analytical relationship between the Y/T ratio and stress concentrations, which will be validated using FEA. To answer this question, first the scope is discussed. Then, the first two parts of the methodology are discussed, the analytical part and the FEA modeling part in Ansys. In the analytical part, several methods are described to find an analytical relationship between the Y/T ratio and the stress field for high strength steel. In the FEA modeling part, a methodology is described, which steps have to be taken in order to model the behavior of specimens with a stress concentration and different material properties. In addition to answer the main question, the third part of the methodology examines the governing parameter for ductile failure, local strain. Then, the fourth part consists of a parametric study to artificially generate different combinations of material properties. Finally, the calibration of the numerical and the validation of the analytical models is discussed. Figure 3.1 shows a schematic visualization of the methodology.

3.1. Scope

In Chapter 2, the scope is already partially defined by limiting it to high strength steel plates subjected to tensile loading. The scope is further restricted by considering only monotonic unidirectional tension. Moreover, circular cutouts of different sizes and double-sided blunt notches are considered as discontinuities. Furthermore, high-strength steels with yield strengths between 690 and 1100 MPa with yield-to tensile ratios between 0.6 and 1 are considered in this study. In addition, the modeled materials are assumed to be isotropic and in-compressible.

3.2. Analytical

The objective of analytical approaches is to approximate elasto-plastic material behavior as accurately as possible. The advantage of the analytical approaches is that the results are obtained very quickly compared to numerical simulation. Also, comparisons between several material property combinations are easily possible. Moreover, the collection of experimental data from standard tensile tests, which are needed for validation of the numerical models, is costly.
There are several approaches to find an analytical relationship between the Y/T ratio and the stress field for high strength steels. The first approach involves rewriting the Stowell equation of Section 2.4 into a form in which the stress field is directly related to the Y/T ratio. In this form, the equation depends only on the nominal quantities. The second approach is to use Neuber's method, which is based on the assumption that the total strain energy density of the pseudo-elastic problem is equal to the total strain energy density of the actual elasto-plastic problem [15]. The third approach is to use an analogy between the Irwin method described in Section 2.4 for a stress concentration instead of a crack tip. This approach yields only the elastic-perfectly plastic solution, which is also considered as the upper bound solution.

3.3. Local strain

To gain further insight into the influence of the Y/T ratio on structural integrity, the local strain at the same location as the stress concentration factor is investigated in addition to the stress concentration factor. The local strain is the governing parameter for ductile failure and therefore very important. More knowledge about local strain could lead to form a good opinion about the influence of the Y/T ratio on structural integrity. Local strain is evaluated via calibrated numerical models and validated analytical models. These analytical models for local strain will be based on the method of Stowell and Neuber.

3.4. Parametric study

In order to investigate the influence of the Y/T ratio in more detail, a parametric study will be carried out. A total of four parameters are investigated. In addition to the Y/T ratio, the yield strength, strain hardening exponent n and strength coefficient K are investigated. The variation of these parameters will provide further insights into the effect on the behavior of the material, as the combination of these parameters with the Hollomon equation will provide the required plastic input to the numerical model. An experimental data set from Bannister will be used to determine feasible combinations of Y/T and the yield strength [2]. The use of these parameters in combination with a relationship between the Y/T ratio, yield strength, and basic stress-strain relationships, can lead to the determination of the strain hardening parameter and the strength coefficient. These values are gradually varied to see the effect on material behavior. The ability to control the parameters will also lead to validation of the analytical models for a wider range of material properties.

3.5. FEA model

In order to validate the analytical results at the end of the research, FEA models of high strength steels are constructed in Ansys software with a stress concentration. For the calibration of the numerical model itself, the experimental standard tensile test data from Appendix A are used. First, material models with different strain hardening models are created for the available experimental results to account for the elasto-plastic behavior. Then, the material models are calibrated to the stress-strain curves of the plain steel specimen and the most suitable method is selected and further applied.

3.6. Validation

Once the numerical model of the plain steel specimen is calibrated, discontinuities can be added to the geometries. These models can be double checked against the experimental data including discontinuities from Appendix A. After calibration of the numerical material model, the influence of the boundary conditions should be checked. This could be checked by looking at the theoretical value of the elastic SCF versus the actual value. If the actual elastic SCF of the model is lower than the theoretical elastic SCF, increasing the size of the model could be a solution to minimize the influence of the boundary conditions and satisfy the Saint-Venant's principle.
The analytical models depending on the stress field and Y/T ratio can be validated with the FEA models, after the validity of the Saint-Venant's principle is checked of the numerical models. This is important because the analytical models of the stress fields use an infinite plate approach where the boundaries are assumed to have no effect on the stress concentration. Once this effect is determined, the influence of the Y/T ratio on the stress field described by the analytical formulation can be validated with numerical results from the FEA models for different Y/T ratios.

Once all the results are collected, they will be evaluated for specific values considering the required design specifications. For example, the lifting appliances regulations of Lloyds, DNV-GL, and Bureau Veritas will be reviewed for the limits therein [21, 33, 39].

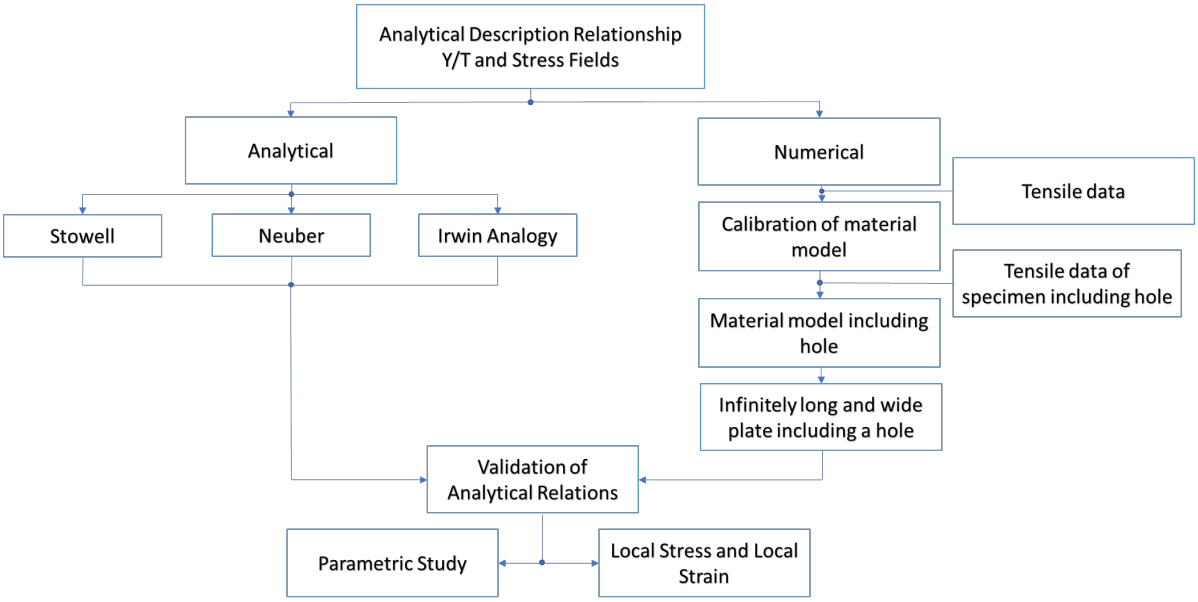

Figure 3.1: Schematic overview of the methodology

4

Analytical method

In order to describe the material behavior in a more general way and to improve its applicability, analytical formulations for the behavior of the stress fields as a function of the Y/T ratio are introduced. First, a relationship between Y/T and the strain hardening exponent n is discussed. Then, Stowell's approach and Neuber's approach are considered based on this relationship. Later, the transition of the elasto-plastic field across the width of the specimen is discussed. After that, the local strain is examined. Finally, the parametric study approach is explained.

4.1. Relation Y/T and hardening parameter n

To achieve relating Stowell's and Neuber's theory to Y/T, a relationship between the strain hardening exponent n and Y/T is needed. This analytical equation is found by Leis and given including essential substeps in Equation (4.1) to (4.7) [17]. Equation (4.1) describes the Hollomon's law.

$$\sigma_{true} = K \cdot \epsilon_{true}^{n} \tag{4.1}$$

Equation (4.2) follows from applying the Considère's equation and rewriting this equation for engineering strain gives Equation (4.3).

$$\epsilon_{u,true} = ln(1 + \epsilon_{u,eng}) = n \tag{4.2}$$

$$\epsilon_{u,eng} = e^{n} - 1 \tag{4.3}$$

An expression for the strength coefficient is found in Equation (4.4) by rewriting Hollomon's law using the Considère equation.

$$K = \frac{\sigma_{u,true}}{n^{n}} \tag{4.4}$$

Substituting the expression for the strength coefficient into Hollomon's law yields Equation (4.5).

$$\frac{\sigma_{y,true}}{\sigma_{u,true}} = (\frac{\epsilon_{y,true}}{n})^{n} \tag{4.5}$$

Rewriting in terms of engineering stresses and strains gives Equation (4.6) and Solving for the engineering yield stress divided by the engineering ultimate tensile stress gives the Leis equation in (4.7).

$$\frac{\sigma_{y,eng} \cdot (1 + \epsilon_{y,eng})}{\sigma_{u,eng} \cdot e^{n}} = (\frac{ln(1 + \epsilon_{y,eng})}{n})^{n} \tag{4.6}$$

$$\frac{\sigma_{y,eng}}{\sigma_{u,eng}} = \frac{1}{1 + \epsilon_{y,eng}} \cdot (\frac{e \cdot ln(1 + \epsilon_{y,eng})}{n})^{n} \tag{4.7}$$

The engineering yield strain, $\epsilon_{y,eng}$, in Equation (4.7) can be approximated by two methods. Hooke's law can be solved for the yield strain. Also, Hollomon's law can be rewritten to Equation (4.8) to estimate the yield strain. These equations can be substituted into Equation (4.7). Combined with the material

and fitting properties of S690, S1100, and S960, given in Chapter 5 in respective Tables 6.1,6.2, and 6.3, the equations for the strain hardening exponent n can be solved. Then, the solved strain hardening exponents can be compared with the strain hardening exponents obtained by the curve fitting procedure described in Sections 6.1 and 6.2. An overview of the strain hardening exponents is given in Table 4.1 for both engineering yield strain approximations.

$$\epsilon_{y,eng,Hollomon} = (\frac{\sigma_{y,eng}}{K})^{(1/n)} \tag{4.8}$$

Table 4.1: Results solving Leis with Hooke's law and Hollomon's law for hardening exponent

Parameter	S690 (K=1090 [-])	S960 (K=1490 [-])	S1100 (K=1625 [-])
Hooke's Law - n	0.041	0.044	0.044
Hollomon's Law - n	0.054	0.061	0.041
Fitted value - n	0.053	0.055	0.037

From Table 4.1, can be concluded that the Leis method with the Hollomon's approximation of the engineering yield strain provides the best agreement for the strain hardening exponent n compared to the fitted value for the hardening parameter. Therefore, this method is used for the Leis equation to relate the strain hardening exponent to Y/T.

4.2. Stowell Applied

In order to establish an analytical relationship between Y/T and the stress concentration factor, Stowell's equation is used and rewritten. This equation describes the stress concentration factor for a circular cutout under uniform tension and is given in Equation (2.15). Here, a is the radius of the circular cutout, r is the distance from the hole center to any point, E_s is the actual secant modulus, $E_{s,\infty}$ is the far-field secant modulus, and θ is the angle between the horizontal axis and the point of interest. An overview of the parameters is shown in a sketch in Figure 2.5. Stowell's method can be rewritten with Hollomon's power law and using an intersection between linear elastic theory and Hollomon's formula. This approach is referred to as "Stowell Applied". Stowell assumes an infinite plate under uniform applied tension with a circular cutout. The plate is assumed to be isotropic and incompressible.

To find the stress concentration factor with input values based only on nominal quantities and material properties, Equation (2.15) must be rewritten, specifically, the ratio $\frac{E_s}{E_{s,\infty}}$. This ratio implies the rate of plasticity of the steel when the yield strength is exceeded. Equation (4.9) is used to rewrite the secant modulus. Here, $E_s \cdot \epsilon$ and $K \cdot \epsilon^n$ are estimates of the stress at a given point on the stress-strain curve.

$$E_s \cdot \epsilon = K \cdot \epsilon^n \tag{4.9}$$

Solving for the secant modulus E_s and rewriting ϵ using Hollomon's law yields Equation (4.10).

$$E_s = K * (\frac{\sigma}{K})^{\frac{n-1}{n}} \tag{4.10}$$

The strength coefficient K could also be rewritten using Equation (4.9) where is assumed that yield stress occurs at the intersection of the elastic region and Hollomon's equation. Therefore, the secant modulus is equal to the Young's Modulus. The result is shown in Equation (4.11).

$$K = E \cdot (\frac{\sigma_y}{E})^{1-n} \tag{4.11}$$

Substituting this expression into Equation (4.9) and dividing by the Young's Modulus because of far-field elasticity, an expression for the ratio $\frac{E_s}{E_{s,\infty}}$ in terms of the stress concentration factor, nominal stress σ_{nom}, yield stress σ_y, and strain hardening coefficient n is obtained given in Equation (4.12). This expression can be substituted into Equation (2.15), resulting in Equation (4.13), and solved numerically

for the stress concentration factor. The strain hardening exponent in this equation can be calculated using Equation (4.7) from Section 4.1. SCF values from 1, full plasticity, up to 3, theoretical elasticity, are considered. The nominal stress is based on the net cross section of a specimen without taking into account the discontinuity.

$$\frac{E_s}{E} = (\frac{\sigma}{\sigma_y})^{\frac{n-1}{n}} = (\frac{\sigma}{\sigma_{ff}} \cdot \frac{\sigma_{ff}}{\sigma y})^{\frac{n-1}{n}} = (SCF \cdot \frac{\sigma_{ff}}{\sigma y})^{\frac{n-1}{n}} \tag{4.12}$$

$$SCF = \frac{1}{2}\left(1 + \frac{a^2}{r^2} - (SCF \cdot \frac{\sigma_{ff}}{\sigma y})^{\frac{n-1}{n}} \cdot (1 + \frac{3a^4}{r^4}) \cos 2\theta\right) \tag{4.13}$$

4.3. Neuber

The elasto-plastic stress concentration factor can also be calculated using Neuber's method. This method is based on the hypothesis that the product of stress and strain in the pure elastic state is equal to the same product [18]. The derivation of Neuber's method for a stress concentration near a hole is shown in Equations (4.14) to (4.19).

$$\sigma_{22} \cdot \epsilon_{22} = \sigma_{elastic} \cdot \epsilon_{elastic} \tag{4.14}$$

$$\epsilon_{22} = (\frac{\sigma}{K_\epsilon})^m \tag{4.15}$$

$$\sigma_{22} \cdot (\frac{\sigma_{22}}{K_\epsilon})^m = \frac{(3 \cdot \sigma_2^0)^2}{E} \tag{4.16}$$

$$\sigma_{22} = (\frac{9 \cdot K_\epsilon^m}{E})^{\frac{1}{m+1}} \cdot (\sigma_2^0)^{\frac{2}{m+1}} \tag{4.17}$$

$$K_t = \frac{\sigma_{22}}{\sigma_2^0} = 3 \cdot (\frac{\sigma_y}{3 \cdot \sigma_2^0})^{\frac{m-1}{m+1}} \tag{4.18}$$

$$m = 1/n \tag{4.19}$$

Here, σ_{22} and ϵ_{22} are the second principal stress and strain, respectively. σ_2^0 is the nominal stress. Neuber assumes unidirectional uniform tension. Therefore, σ_{22} and ϵ_{22} are used in the derivation. The classical solution of the equation is obtained when the nominal stress is equal to $\frac{\sigma_y}{3}$. The stress concentration factor is equal to the theoretical value of 3 when this is used. The strain hardening exponent can be calculated using Leis' equation in Section 4.1. Using Neuber's method requires an if statement to constrain outputs greater than the theoretical elastic SCF equal to 3.

4.4. Transition elasto-plastic field

The changing extent of the plastic zone should be considered when analyzing the SCF including the strain hardening behavior as a function of the width of the geometry (r/a). Irwin came up with a method to implement this in crack analysis [1]. If this method is used as an analogy and implemented for stress concentrations, Equation (4.20) can be used to correct for the changing plastic zone at $\theta = \pi/2$ according to the maximum value.

$$\frac{R}{a} = \frac{r}{a} - (\frac{r_p}{a} - \frac{r_y}{a}) \tag{4.20}$$

Here, r_y is the first order estimate of the plastic zone and can be calculated by solving Equation (4.21) [41]. This leads to Equation (4.22).

$$\frac{\sigma_\theta}{\sigma_{ff}} = 1 + \frac{1}{2} \cdot \frac{a^2}{r_y^2} + \frac{3}{2} \cdot \frac{a^4}{r_y^4} \tag{4.21}$$

$$\frac{a}{r_y} = \sqrt{-\frac{1}{6} \pm \frac{1}{3}\sqrt{-\frac{23}{4} + 6 \cdot \frac{\sigma_\theta}{\sigma_y}}} \tag{4.22}$$

The estimate of the second order plastic zone, r_p can be calculated by solving the energy balance given in Equation (4.23). $\frac{r_p}{a}$ can be determined shown in Equation (4.24).

$$\sigma_y \cdot r_p = \int_0^{r_y} \sigma_\theta dr \tag{4.23}$$

$$\frac{r_p}{a} = \frac{\sigma_{ff}}{\sigma_y} \cdot (\frac{r_y}{a} - \frac{1}{2} \cdot \frac{a}{r_y} - \frac{1}{2} \cdot (\frac{a}{r_y})^3) + 1 \tag{4.24}$$

To calculate the plastic SCF including hardening using the Irwin approach, the reformulated R/a from Equation (4.20) can be substituted into Equation (4.13) in Stowell Applied. This gives the solution including shifts of the extent of the plastic zone. Calculating the elastic-perfectly plastic solution, the R/a can be substituted back into Equation (4.21).

4.5. Local strain

If the research question can be answered, the influence of the Y/T ratio on the stress field can be assessed. A great addition would be to relate the SCF to the local strain, since the local strain is the governing parameter for ductile failure. To achieve this relationship, Equation (2.15) of Stowell can be solved for the local strain ϵ. A simplified situation at the maximum stress with $r/a = 1$ and $\theta = \pi/2$ yields Equation (4.25). Analysis of this equation gives an indication of the interrelated behavior. A decrease of the plastic SCF would lead to an increase in local strain. On the contrary, a relative increase in the plastic SCF leads to a decrease in the local strain. This will be further investigated in the results in Chapter 7.

$$\epsilon_{local} = ((\frac{1}{2} \cdot SCF - \frac{1}{2}) \cdot \frac{E}{K})^{\frac{1}{n-1}} \tag{4.25}$$

4.6. Parametric study

A parametric study is desired to extensively look into the governing parameters of the elasto-plastic behavior of high strength steels. The four governing parameters are the Y/T ratio, yield strength, strain hardening exponent n, and strength coefficient K. The combination of these parameters leads to a description of the strain hardening behavior according to the Hollomon equation. Varying these separately gives further insight into the influence of these parameters. These parameters are interrelated to each other. Thus, when the Y/T is varied, the yield strength remains constant and the tensile strength is varied, but the strain hardening exponent and the strength coefficient also vary with Y/T. The same is true for varying the yield strength where the Y/T ratio is kept constant. If the strain hardening exponent is varied, the strength coefficient is kept constant and Y/T and yield strength vary with the strain hardening exponent. The same method is used for the strength coefficient.

A relationship between Y/T and the yield strength is used to provide the required information. Data from Bannister within SINTAP provides much information on the relation between the yield strength and the Y/T ratio [2]. This data is based on a large set including high strength bainitic steels and austenitic stainless steels among others. Bannister fitted a conservative upper bound that resulted in a relationship between the Y/T ratio and the yield strength shown in Equation (4.26). Using this upper bound in combination with the data and fitting a lower bound results in Figure 4.1. The lower bound is constructed roughly by trial and error resulting in Equation (4.27) [41].

$$\frac{Y}{T} = \frac{1}{1 + 2(150/\sigma_y)^{2.5}} \tag{4.26}$$

$$\frac{Y}{T} = \frac{1}{1 + 2(150/\sigma_y)^{1.4}} \tag{4.27}$$

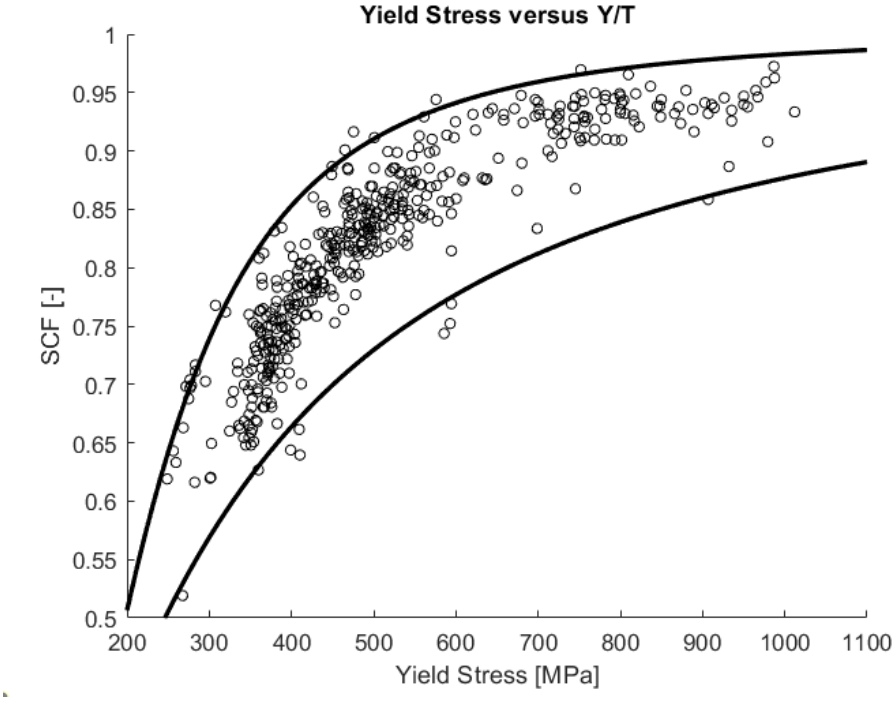

Figure 4.1: Experimental data yield strength versus Y/T ratio from SINTAP [2]

Besides the relation between the Y/T ratio and the yield stress, a relation between the Y/T ratio and the strain hardening exponent is needed. Leis's Equation (4.7) provides this relationship. When the Y/T ratio is varied, or the yield stress is varied, it affects the value of the strain hardening exponent according to this relationship.
The strength coefficient K is also closely related to all parameters. Two approaches can be used to determine this coefficient. The first approach consists of equating Hooke's law with Hollomon's law at the yield point and solving for K. This is shown in Equation (4.28). The second approach uses the Considère equation, used for diffuse necking in an uniaxial test, to determine the parameters at the ultimate tensile strength [4]. This leads to Equation (4.29) using the true ultimate stress. The derivation of this equation is discussed in Section 4.1. The second approach will be more accurate because Hollomon's law uses in this method higher strains at ultimate tensile strength in stead of yield strength. Therefore, the second method is more accurate for higher strains and will therefore be used for the parametric study.

$$\epsilon_y \cdot E = K \cdot \epsilon_y^n \tag{4.28}$$

$$K = \frac{\sigma_{u,true}}{n^n} \tag{4.29}$$

As discussed, the parametric study is divided into four parts where Y/T, yield strength, strain hardening parameter n, and strength coefficient K are varied. With a constant value of 976.25 [MPa] for the yield strength, the values equal to 0.6, 0.86, 0.91, and 0.96 are chosen for the changing study of Y/T as shown in Figure 4.1. For the change in yield strength, values equal to 690, 960, and 1100 [MPa] are chosen with a Y/T equal to 0.95 which also fits in the bounds in Figure 4.1. The values for n are chosen equal to 0.0001, 0.02, 0.0282, 0.04, 0.05, and 0.06. 0.0282 is the original value here which fits the rest of the parameters. K is taken equal to 1117. In terms of parametric study of parameter K

values equal to 1000, 1117, and 1200 are used. Here, $K = 1117$ is the original value for K.
For each parameter the following plots are made; SCF vs r/a, SCF vs normalized nominal stress, and the normalized peak strain versus the normalized nominal stress. Analysis of the results provides further insights into the influence of each parameter on the stress field, elasto-plastic SCF, and the local peak strain.

5

Numerical simulations

In this chapter, numerical simulations of standard tensile tests on high strength steel specimens with discontinuities are performed. Specimens with symmetrically aligned notches equal to 2 mm and 4 mm and specimens with circular cutouts with varying hole sizes are simulated. The aim of this chapter is to calibrate the numerical models created in Ansys. First, the layouts of the test specimens are discussed, followed by a discussion of various aspects related to Ansys. At the end, a method is described to compare numerical results to experimental tensile test results. A static solver with an iterative solver based on the Newton-Raphson method is used for the numerical simulations in Ansys. The extracted stresses from Ansys are Von Mises stresses.

5.1. Specimen Types

As discussed in Section 2.5, experimental data from standard tensile tests are available from Stofregen [35] and VTT [13]. This section describes the design of the specimens that will be used later in the numerical simulation.

5.1.1. Stofregen specimen

Standard tensile data of S690 and S1100 steel conducted by Stofregen are given in Appendix A. The layout for the plain steel specimen is shown in Figure 5.1. The specimens with symmetrically aligned notches of 2 mm and 4 mm are shown in Figures 5.2 and 5.3, respectively. The loading of the standard tensile test is applied to the vertical edges. It is noticeable that the gauge length L_0 differs and is increased for notched specimens, as this quantity depends on the cross-sectional area of the specimen, which is increased for the notched specimens. The gauge length is calculated as $5.65 \cdot \sqrt{S_0}$ according to EN 6892-1 [24]. Here, S_0 is the initial cross-sectional area of the specimen. The thickness of the specimen is 12 mm.

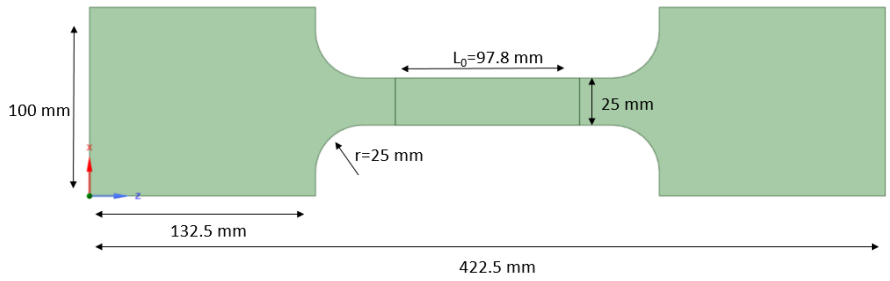

Figure 5.1: Stofregen standard tensile test specimen

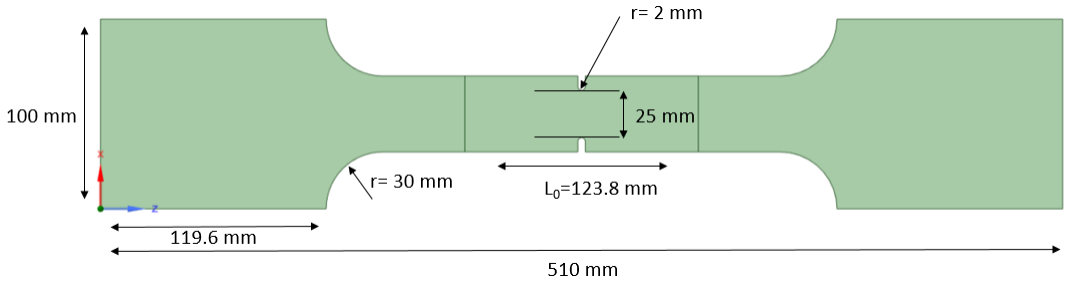

Figure 5.2: Stofregen standard tensile test specimen with 2 mm notch

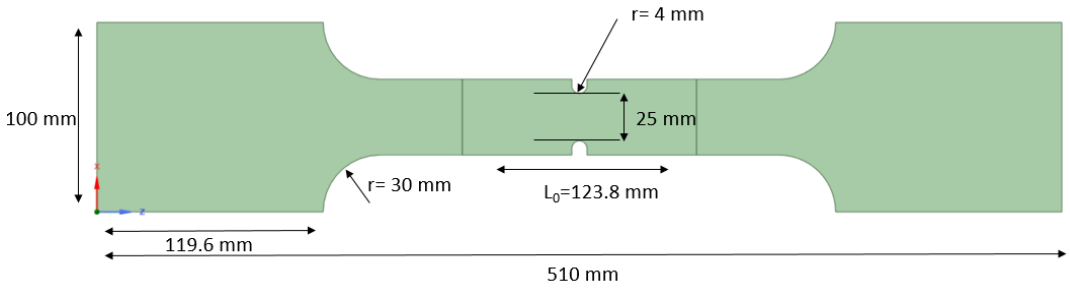

Figure 5.3: Stofregen standard tensile test specimen with 4 mm notch

5.1.2. VTT specimen

Standard tensile data of S960 steel performed by VTT are given in Appendix A. The specimens are provided with a circular cutout that varies in size between 0 to 40 mm, as shown in Figure 5.4. The thickness of the specimen is 8 mm.

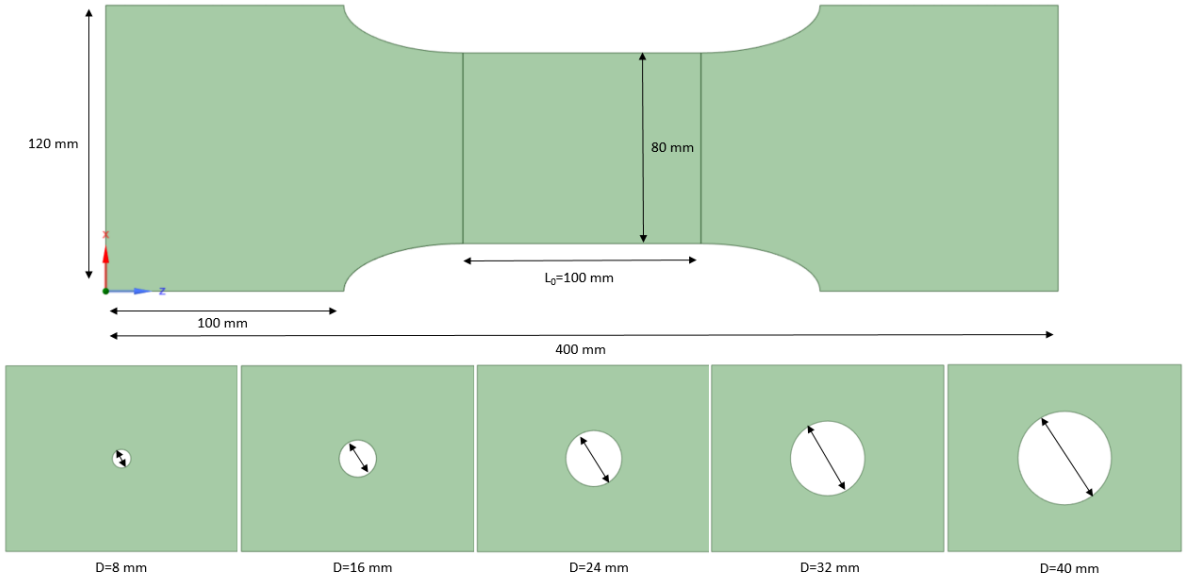

Figure 5.4: VTT standard tensile test specimen with varying circular cutouts

5.2. Calibration material models

Calibrating of material models is important as the numerical simulation should represent the material behavior as realistically as possible. Numerical simulation is performed for models that behave in an elasto-plastic manner. The behavior of standard tensile tests for the plain steel specimen in the experiment is numerically approximated. The stress-strain behavior of the standard tensile test is approximated using various methods that describe the hardening behavior. After calibration, the geometry of the specimen can be changed, extending the applicability of the numerical model. In addition, specific behavioral parameters such as stresses and displacements can be extracted from a calibrated numerical model.

5.2.1. Methods describing hardening behavior

Different methods can be used to describe the non-linear hardening behavior of a specimen in a standard tensile test. For the numerical simulation of a notched specimen, a method proposed by Stofregen, the Ramberg-Osgood method, and Hollomon's method are used and balanced against each other [35]. The Stofregen method converts the engineering stress and strain values to true stress strain values from the engineering strain at yield up to an engineering strain equal to 0.04 according to equations (5.1) and (5.2). For strains greater than or equal to 0.04, Hollomon's law is used, which is explained further.

$$\sigma_{true} = \sigma_{engineering} \cdot (1 + \epsilon_{engineering}) \tag{5.1}$$

$$\epsilon_{true} = ln(1 + \epsilon_{engineering}) \tag{5.2}$$

The Ramberg-Osgood method is also an empirically based approximation for strain hardening behavior. Equation (5.3) describes this method. Here, ϵ is the dimensionless strain, σ is the stress in N/mm^2, E is the Young's Modulus in N/mm^2, H is the strength coefficient in N/mm^2 , and n is the dimensionless strain hardening exponent. Hollomon's law is described by Equation (2.17) in Section 2.3.

$$\varepsilon = \frac{\sigma}{E} + \left(\frac{\sigma}{H}\right)^{1/n} \tag{5.3}$$

$$\epsilon = \frac{\sigma}{E} + 0.002 \cdot (\frac{\sigma}{\sigma_y})\frac{1}{n} \tag{5.4}$$

The description of the non-linear hardening behavior requires fitting the empirically based methods of Ramberg-Osgood and Hollomon methods to the actual data of the standard tensile test. The Ramberg-Osgood method can rewritten to equation (5.4) if the yield stress is assumed to be at 0.2 % offset strain. The fit parameter n can then be determined by solving this equation for n. Equation (5.3) can be used with H and n as the fitting parameters which can be changed iteratively. Typically, the Ramberg-Osgood method is used up to the ultimate strength where Hollomon's law is then fitted to this point using the Considère equation to determine n and then solving K to determine the strength coefficient. The Considère equation is described in Section 2.1. Using Hollomon's law alone requires an iterative fitting of the parameters K and n. The obtained data is used as a plastic input to Ansys. Here, the plastic strain input is equal to the total strain minus the elastic strain.

5.2.2. Boundary conditions

In order to obtain a numerical model representing an actual standard tensile test, appropriate boundary conditions should be applied. These boundary conditions consist of constraining movements and applying displacements. Figure 5.5 shows an applied remote displacement on the solid VTT specimen. A remote displacement is chosen over an applied load because it best simulates reality. Due to the fact that an elasto-plastic simulation must be performed, an applied load would not be suitable instead of a remote displacement. This is because according to the experiments shown in Appendix A, the force will be more or less constant as the material yields. If this is modelled numerically with an applied force, no additional strain will occur in the constant part. A constantly increasing load will cause the material to yield, resulting in a more or less constant force in the plastic part. For a purely elastic model, an applied load would be sufficient because the load is constantly increasing. To simulate the standard tensile test , the right edge of the specimen is clamped in the X and Y directions in addition

to the remote displacement. Moreover, the rotations about the X, Y , and Z directions are set equal to zero. The applied boundary conditions on the left edge do not allow any movements in the X, Y, and Z direction. Also, the rotations about the X, Y, and Z directions are limited to zero. Moreover, the applied boundary conditions behave as deformable as this is the most realistic representation and deformable boundary conditions result in a perpendicular reaction force. Furthermore, it is important to consider the influence of the edges on the stress concentration around a discontinuity like a circular cutout. The edge at the width of the specimen could have an influence on the stress field if the width to diameter ratio is not high enough. This will be evaluated in the results in Chapter 7.

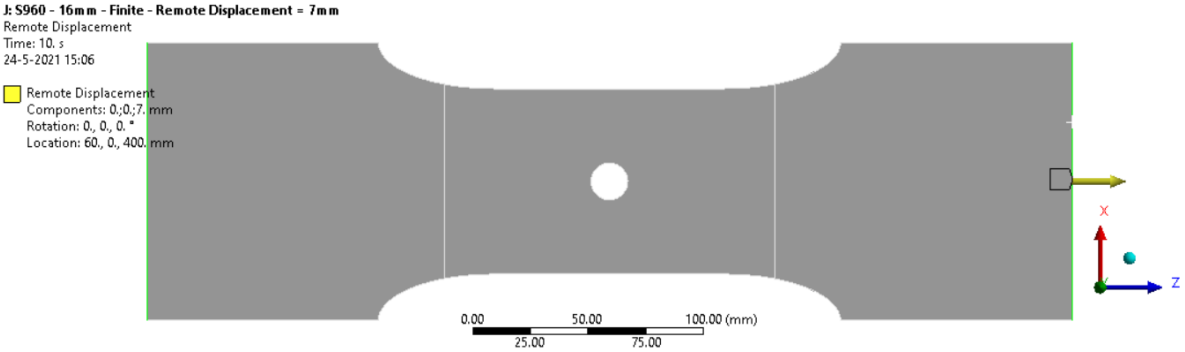

Figure 5.5: Applied boundary conditions on VTT specimen

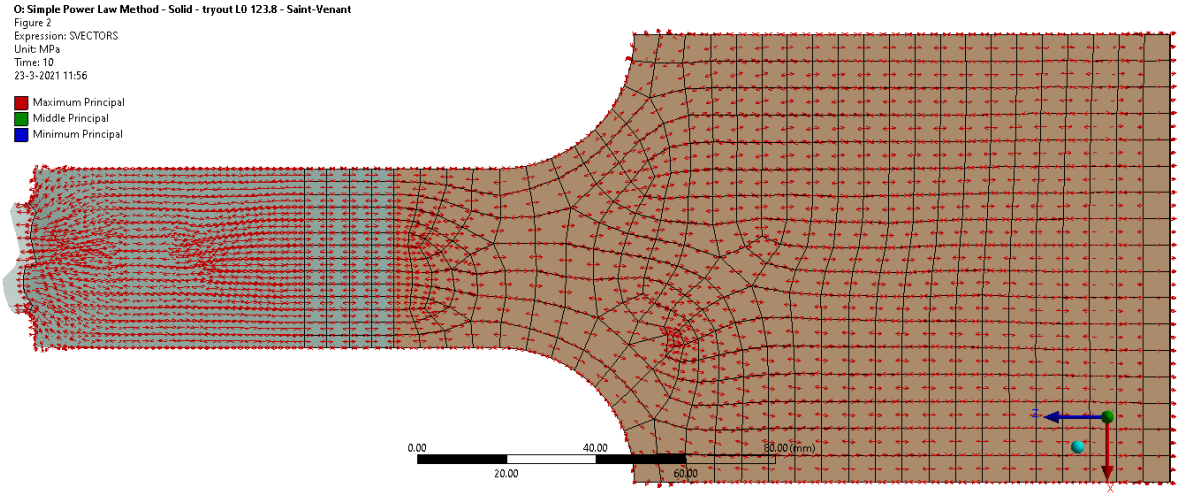

Figure 5.6: Vector plot S690 2 mm notch

The effect of finite width and finite length on the behavior of the material should also be evaluated. A finite width could have an effect on the stress flow around a discontinuity. An empirical relationship is available in the literature to evaluate the influence of the diameter over the width ratio of the specimen when a circular cutout is present in the specimen. This relationship is shown in Figure 5.7. A value close to 0 for a specimen with a circular cutout would give the best agreement with the theoretical stress concentration factor. This means that the width should be significantly greater than the discontinuity to prevent any influence. In order to eliminate the influence of the boundary conditions as much as possible and at the same time to limit the computation time, a scaling factor of 6 is chosen. Further increasing the scaling factor would reduce the effect of the boundary conditions but would significantly increase the computation time.

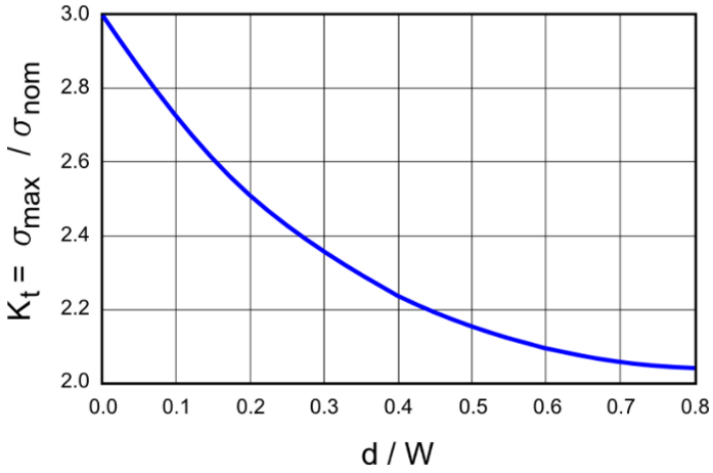

Figure 5.7: Empirical relation diameter/width ratio [22]

5.2.3. Convergence study

The choice of the mesh size has a major impact on the accuracy of the numerical model results. In general, a reduced mesh size leads to more accurate results up to the point of convergence. In this study, a change in peak stress of less than 1 % is assumed to be convergent. The advantage of choosing the mesh size corresponding to the first convergent solution is the reduced computation time. This is because a reduced mesh size leads to an increased computation time. Moreover, this leads to an almost identical result compared to a highly reduced mesh size.
In this study, a convergence study is performed for a double-sided 2 mm notch. For a finite notch like this, a converging value for the peak stress is expected with a decreased mesh size. The result is shown in Figure 5.8. A mesh size of 2 mm is chosen as sufficient to achieve a converging peak stress corresponding to a 0.2 % change in peak stress. A maximum mesh size of 2 mm is used for modelling in areas of interest such as stress concentration. This is also applied to the mesh size in the through-thickness direction. Such a refinement of the mesh in areas of interest is shown in Figure 5.9. Here, a refinement in the thickness direction and around the circular cutout is shown.

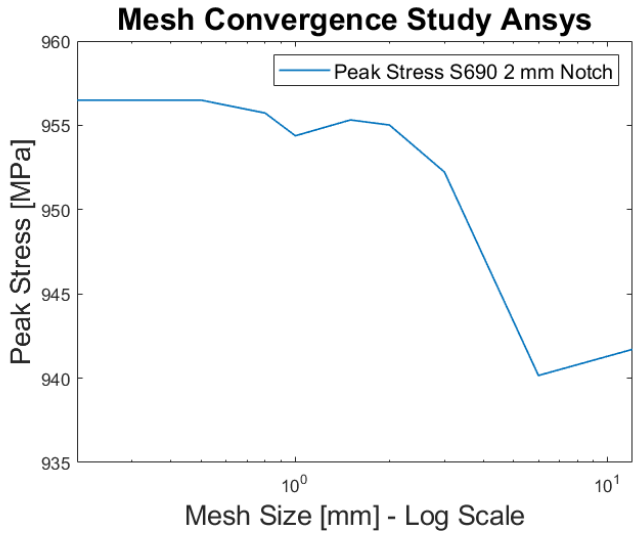

Figure 5.8: Convergence study with x-axis on log-scale

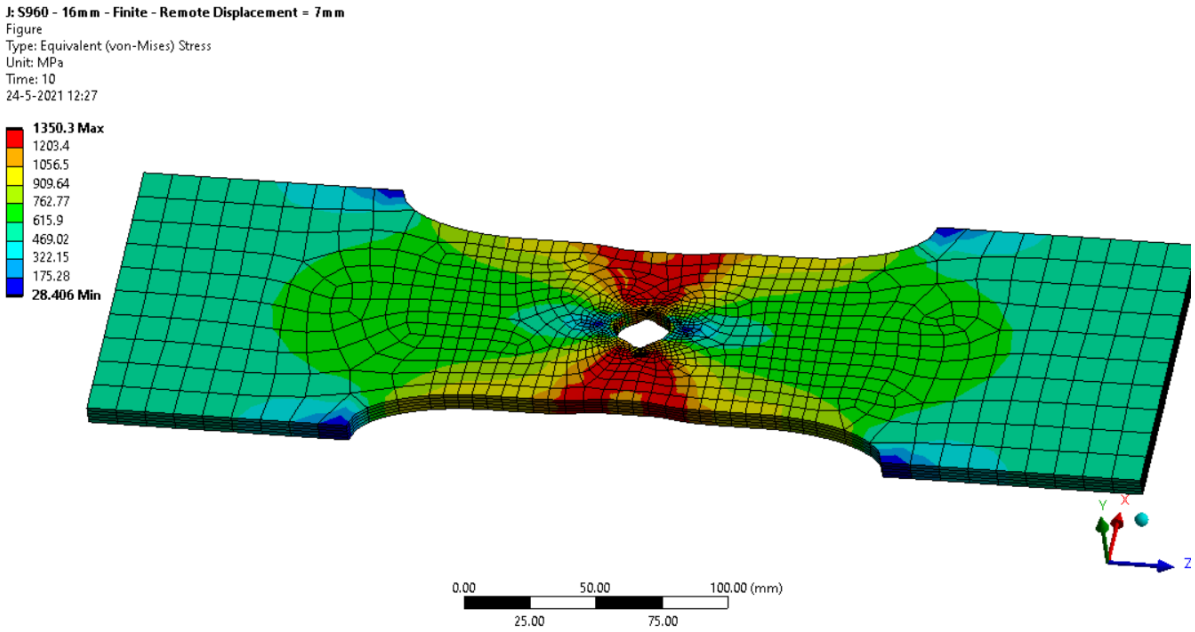

Figure 5.9: Ansys equivalent stress solid VTT specimen 16 mm cutout

5.3. Comparison to experimental values

In order to compare the results from the numerical simulation in Ansys, certain steps need to be performed. In a standard tensile test according to the standards of ISO, the stress is equal to the force in the Z-direction divided by the initial cross-sectional area [24]. Therefore, the force in Z-direction should be extracted from the results of the numerical simulation and divided by the initial area. According to the standard ISO, the strain is the strain measured with respect to the gauge length L_0. In Ansys, this elongation can be calculated by subtracting the displacements of the edges of the gauge length and dividing this value by the original gauge length.

6

Calibration and validation

This chapter discusses the calibration of the numerical models and validation of the analytical models. First, the numerical models are calibrated with experimental tensile data. Then, the Stowell and Neuber models are validated with the calibrated numerical models. Finally, the method of the parametric study will be validated.

6.1. Stofregen material models

The fitting parameters for the Stofregen method, Ramberg-Osgood method and the Hollomon method are given for S690 and S1100 in Tables 6.1 and 6.2, respectively. These parameters result in an approximation of the plain steel behavior of the material in the standard tensile test. The fitting results for S690 and S1100 steel are shown in Figures 6.1 and 6.2, respectively.
All the approximation methods used give a good fit and hence the proposed material models are calibrated with the given fitting parameters. With the final goal in mind to formulate an analytical relationship between Y/T and a stress field, Hollomon's law will end up being the simplest application in the analytical solution. Therefore, this approximation method is preferred for further research. The Ramberg-Osgood method is more difficult to apply in analytical derivations because of the complicated equation. The Stofregen method is generally not applicable when all data are not available, since this method is based only on the direct conversion of engineering values to true values.

Table 6.1: S690 fitting parameters

	Value	**Unit**
Steel grade	S690	[-]
Youngs Modulus	210	[GPa]
σ_{yield}	850	[MPa]
σ_{UTS}	890.1	[MPa]
Y/T	0.955	[-]
$K_{Stof-Hol}$	1107	[-]
$n_{Stof-Hol}$	0.057	[-]
n_{RO}	98	[-]
K_{RO-Hol}	1178	[-]
n_{RO-Hol}	0.08	[-]
K_{Hol}	1090	[-]
n_{Hol}	0.053	[-]

Table 6.2: S1100 fitting parameters

	Value	**Unit**
Steel grade	S1100	[-]
Youngs Modulus	210	[GPa]
σ_{yield}	1247	[MPa]
σ_{UTS}	1369	[MPa]
Y/T	0.91	[-]
$K_{Stof-Hol1;2}$	1659;1591	[-]
$n_{Stof-Hol1;2}$	0.045;0.03	[-]
n_{RO}	27	[-]
K_{RO-Hol}	1620	[-]
n_{RO-Hol}	0.037	[-]
K_{Hol}	1625	[-]
n_{Hol}	0.037	[-]

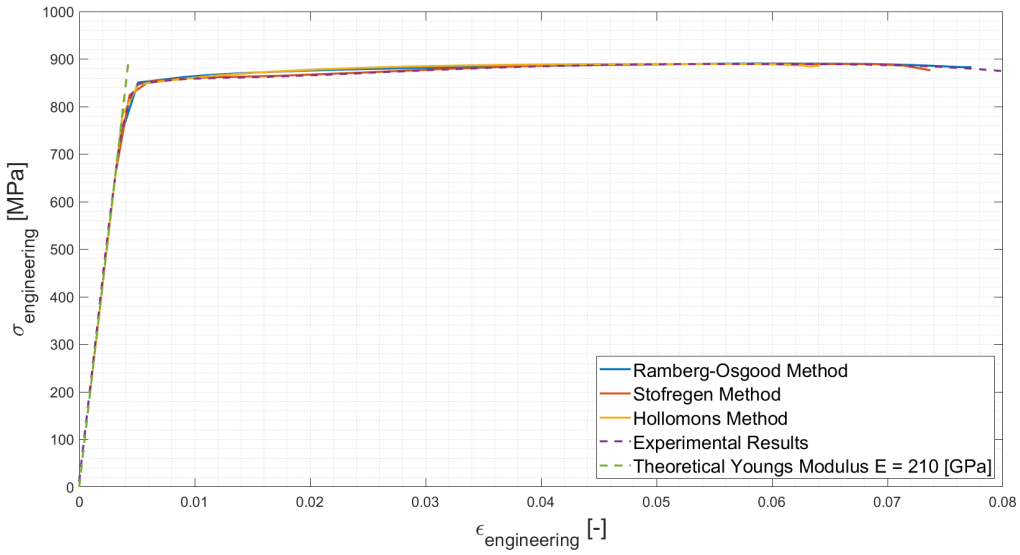

Figure 6.1: Engineering stress as a function of strain approximation methods - Stofregen S690 plain

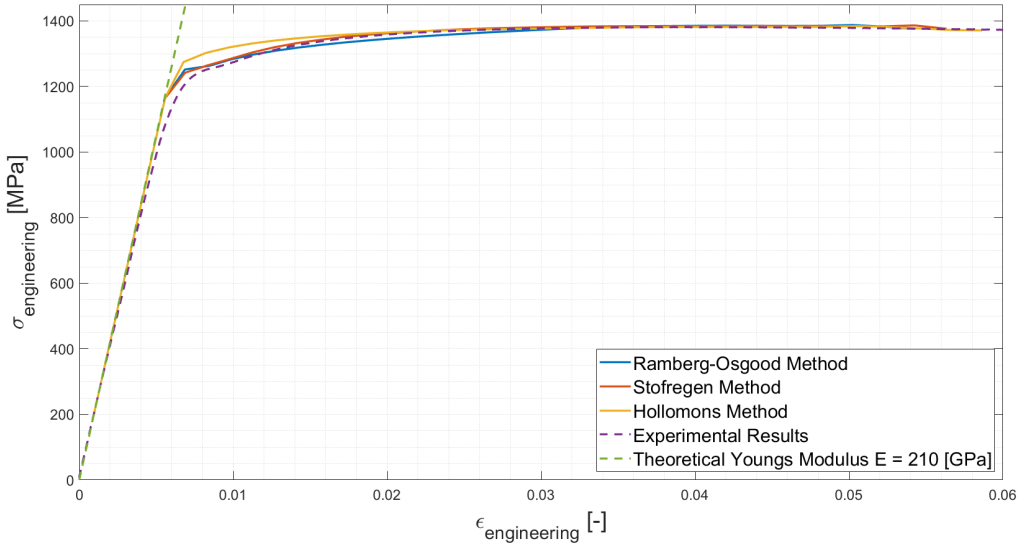

Figure 6.2: Engineering stress as a function of strain approximation methods - Stofregen S1100 plain

Since the engineering stress-strain curve of the numerical simulation shows good agreement with the experimentally determined stress-strain curve, the material models of S690 and S1100 are calibrated. Therefore, the geometry of the numerical model can be changed, but the input parameters must be kept constant. A comparison of the numerical engineering stress-strain curve for S690 with a notch of 2 mm and 4 mm with the experimental stress-strain curve is shown in Figures 6.3 and 6.4, respectively. For the material S1100 with a notch of 2 and 4 mm, the comparative plots are shown in Figures 6.5 and 6.6. The figures corresponding to geometries with discontinuities show good agreement between the numerical approximation and the actual experimental results. A better agreement is obtained for S690 than for the S1100 material. This is in agreement with the conclusion of Stofregen [35]. It is also noteworthy that the numerical solution does not fail. This can be explained by the fact that no failure criterion is added to the numerical model. The notched specimens show a lower failure strain, which can be explained by the present SCF as a result of the discontinuity, causing the material to fail in an earlier stage.

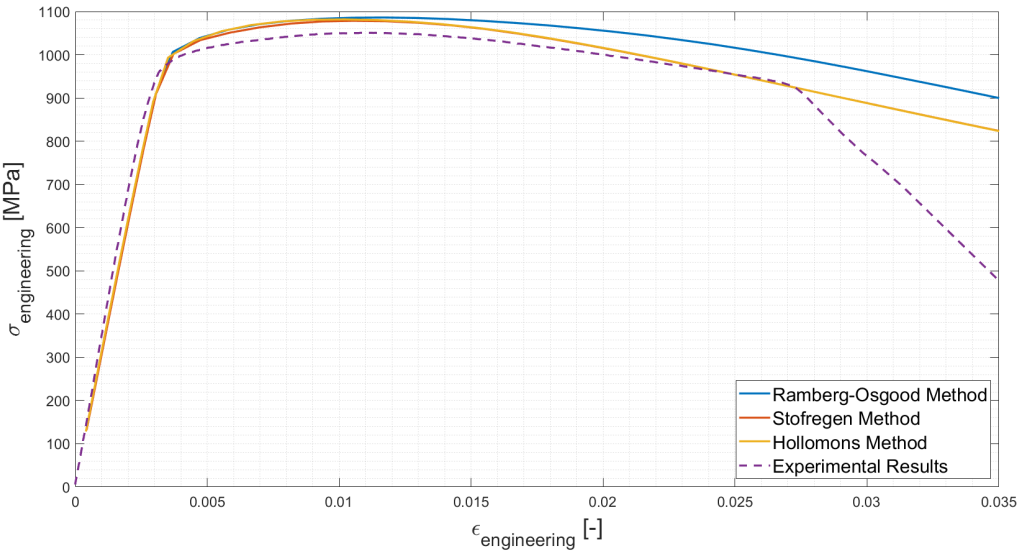

Figure 6.3: Engineering stress as a function of strain approximation methods - Stofregen S690 2 mm notch

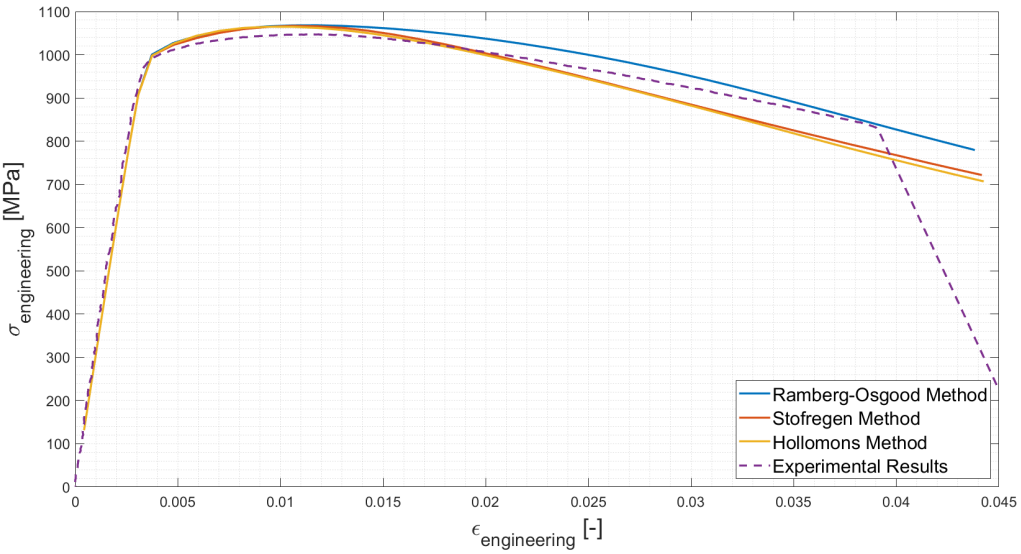

Figure 6.4: Engineering stress as a function of strain approximation methods - Stofregen S690 4 mm notch

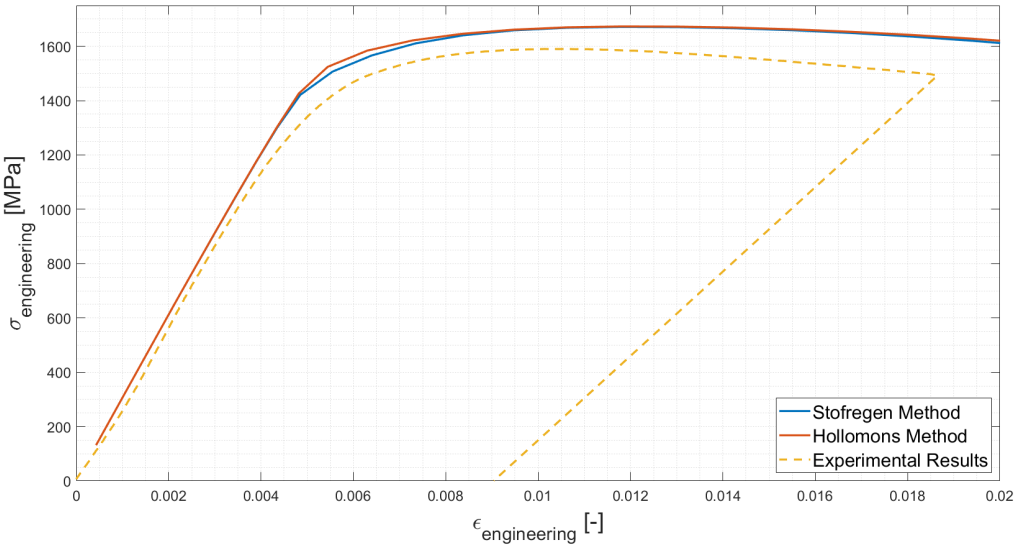

Figure 6.5: Engineering stress as a function of strain approximation methods - Stofregen S1100 2 mm notch

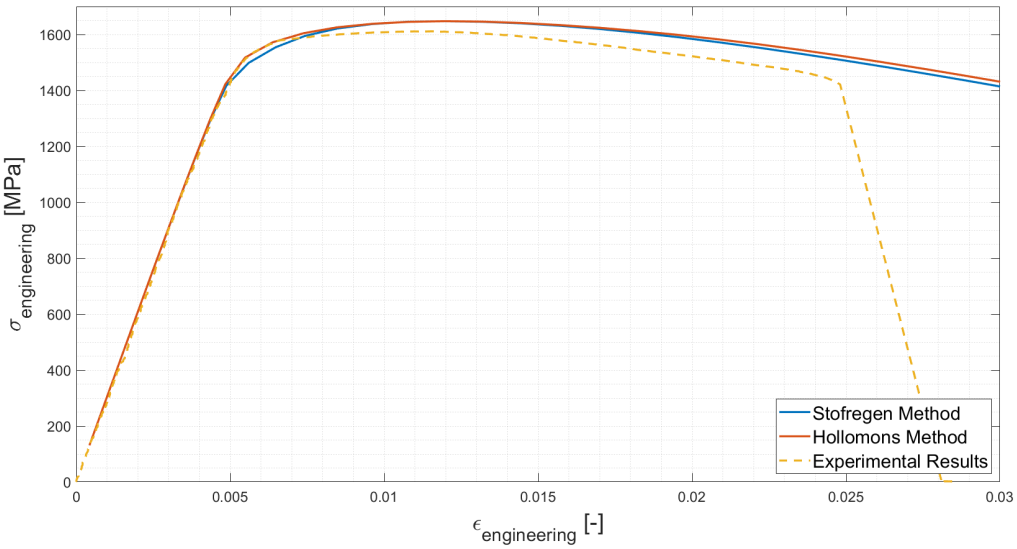

Figure 6.6: Engineering stress as a function of strain approximation methods - Stofregen S1100 4 mm notch

6.2. VTT material model

As discussed in Section 6.1, Hollomon's law is used as an approximation method for the hardening behavior of the numerical model. The fitting parameters for Hollomon's law can be found in Table 6.3. These parameters result in a fit shown in Figure 6.7 for plain steel, which leads to calibration of the material model based on the plastic input of Hollomon's law. Figure 6.8 shows the numerical results in terms of force versus elongation for the different sized cutouts compared to the experimental results from VTT. This choice was made to show all the data in one graph without overlapping results. Overlapping results would be present because of the reduced area due to the hole. Notable in this figure is that a decreasing slope in the elastic part results from an increase in hole diameter. This can be explained by an increase in strain due to an increasing hole diameter. The stress in the elastic part is defined by Hooke's law, stress equals Young's modulus times engineering strain.
Hollomon's law shows a good fit for the S960 plain steel specimen. The agreement between numerical and experimental results for the variable cutout size is also good.

Table 6.3: S960 Fitting parameters

	Value	**Unit**
Steel grade	S960	[-]
Youngs Modulus	210	[GPa]
σ_{yield}	1084	[MPa]
σ_{UTS}	1190.8	[MPa]
Y/T	0.91	[-]
K_{Hol}	1490	[-]
n_{Hol}	0.055	[-]

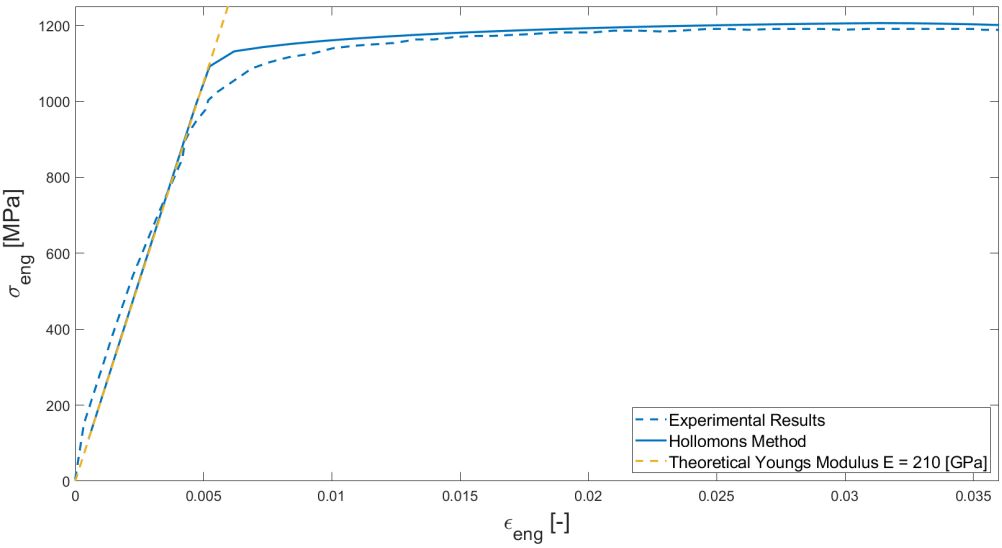

Figure 6.7: Engineering stress as a function of strain Hollomon's law - VTT S960 plain

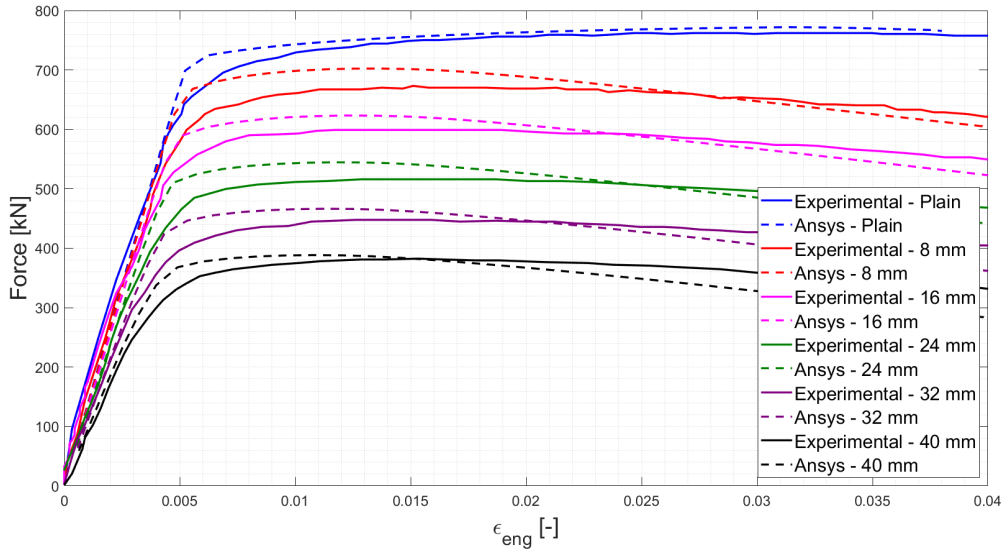

Figure 6.8: Engineering force as a function of strain Hollomon's law - VTT S960 specimen with a circuluar cutout with varying diameter of 0-40 mm

6.3. Analytical models

The analytical equations are validated by evaluating a specific point on the specimen. This point is evaluated at $r = a$ and $\theta = \frac{\pi}{2}$. A schematic representation of this location can be seen in Figure 6.9. This location is chosen because it assigns the highest value to the stress due to the effect of the discontinuity. Furthermore, the theoretical stress concentration factor for a circular cutout under uniform tension is known and equal to 3 at this location.

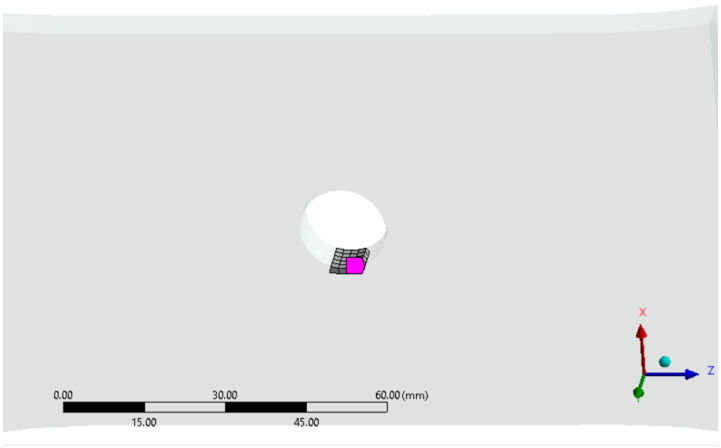

Figure 6.9: Element selection at $\theta = \pi/2$ and a/r=1

To determine the value of the SCF, the maximum stress of the selected elements is divided by the nominal stress. The nominal stress is equal to the force in the Z-direction divided by the initial net cross-sectional area of the specimen without taking into account a discontinuity. This value is plotted against the normalized nominal stress. This stress is normalized to the yield stress as this is useful for comparison purposes. The numerical material models of S690, S960, and S1100 are calibrated in Chapter 5. The fitting parameters of these material models are applied to the circular cutout specimen of VTT. The comparison of the different analytical approaches results in Figures 6.10 to 6.12, which represent the validation of the analytical models by comparing them with the calibrated material models of S690, S960, and S1100. The analytical models indicate a value of 3 at $\frac{\sigma_{ff}}{\sigma_y} = 0.33$, which is the same as the theoretical value. Originally, these analytical relations would lead to vertical asymptotic behavior. However, “if statements” are added to these relations which equate exceeding values of the elastic SCF to the theoretical value of 3.
The figures show a very good agreement between the numerical simulations and the analytical approximation. In particular, very good agreement is obtained for the materials with a relatively low Y/T ratio. Remarkable is the left hand side of the plots where the elastic stress concentration factor is constantly equal to 3, which can be explained by the material behaving elastically. A value of $\frac{\sigma_{ff}}{\sigma_y}$ equal to 0.33 indicates the onset of yielding. The SCF drops to a value close to 1, indicating global yielding. The elastic-perfectly plastic solution for the Irwin, Neuber, and Stowell Applied approaches is discussed in the results in Section 7.2.

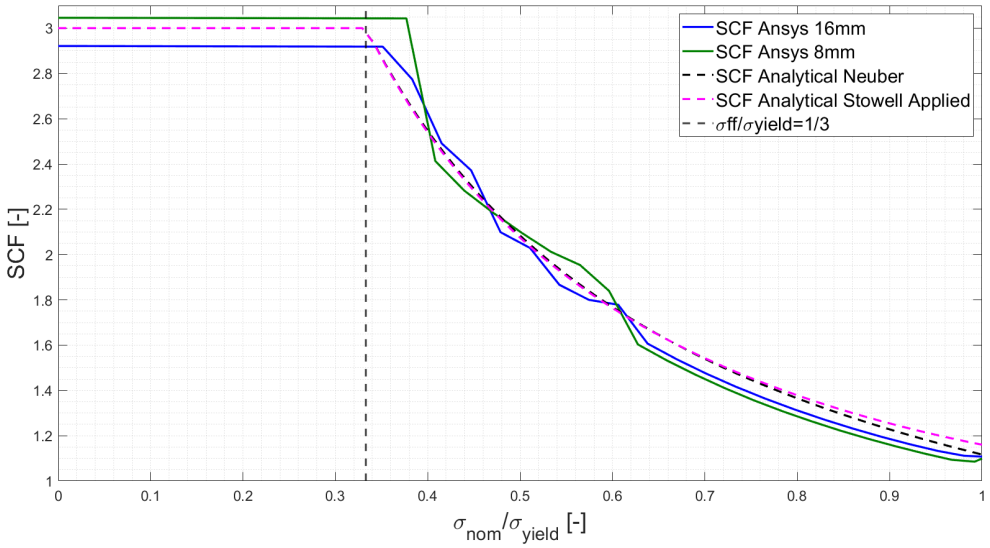

Figure 6.10: S690 SCF vs normalized nominal stress at $\theta = \pi/2$ and a/r=1

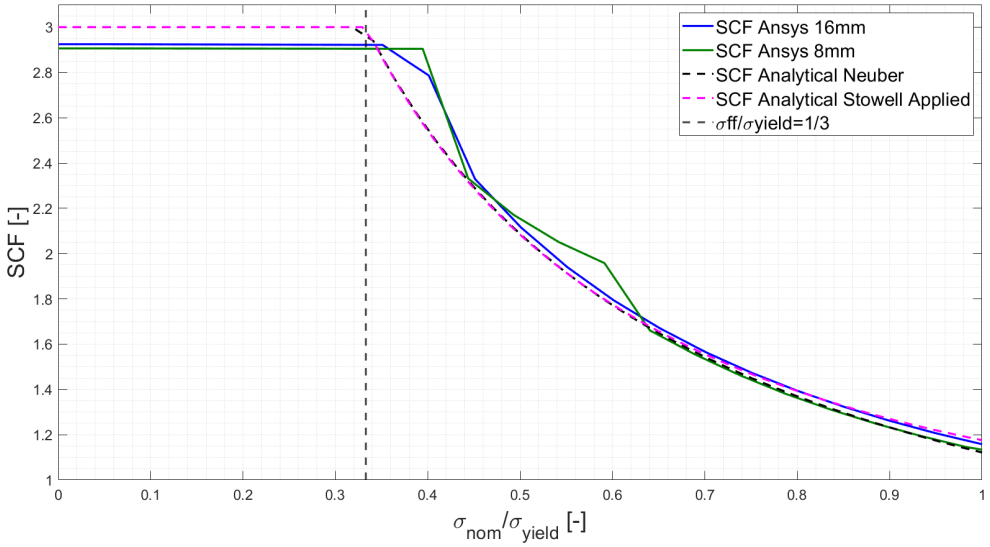

Figure 6.11: S960 SCF as a function of normalized nominal stress at $\theta = \pi/2$ and a/r=1

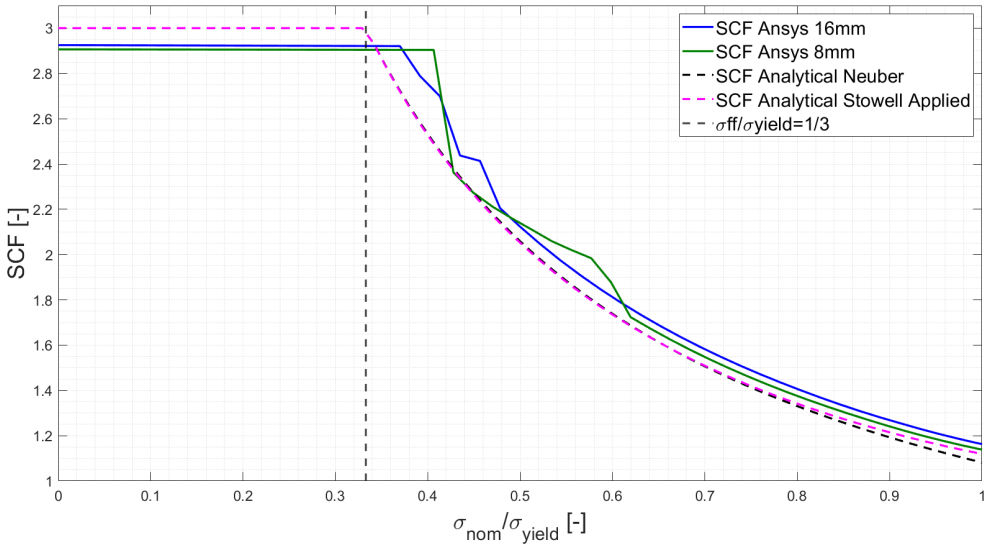

Figure 6.12: S1100 SCF as a function of normalized nominal stress at $\theta = \pi/2$ and a/r=1

6.4. Parametric study

Separate validation apart from equations used in the parametric study is not required. This is because the parametric study is partially based on existing experimental data from Bannister. Moreover, the equations used are already validated in the literature or like the Leis equation mathematically described in the report in Section 4.1. Also, the Hollomon method, which describes the elasto-plastic behavior of the steel, is validated for S690, S960, and S1100 in Chapter 5. Furthermore, only one parameter is varied at a same time, so the relative error between the varied parameters will be zero. Besides these arguments to avoid a separate validation an additional validation is done.

This additional validation consists of reconstructing the material properties of the already calibrated material model of S960 steel in Section 6.2 with a circular cutout under uniform tension. The value for yield strength and ultimate tensile strength are used to calculate the strain hardening exponent and the strength coefficient via the equations described in the parametric study. The strength coefficient is calculated via the second method, which is considers large strains. The plastic input for the multi- linear isotropic hardening is generated using the Hollomon's law for FEA in Ansys. The result of the simulation with the input values obtained via the parametric study method is shown in Figure 6.13. This plot is part of the plot in Section 6.1 Figure 6.8 which gives an overview of all hole sizes of VTT. The difference is the added black dashed curve for the parametric study fit. This shows a very good approximation to the numerical data. A misfit in the elastic part is confirmed like in Section 6.1. This could be explained by a possible bending during the experiment or anisotropic behavior of the steel specimen. This validation offers the possibility to generate input data for elasto-plastic numerical models with relative ease. A combination of yield strength and Y/T can be chosen according to Bannister's data and the strain hardening exponent and strength coefficient can be calculated with given equations.

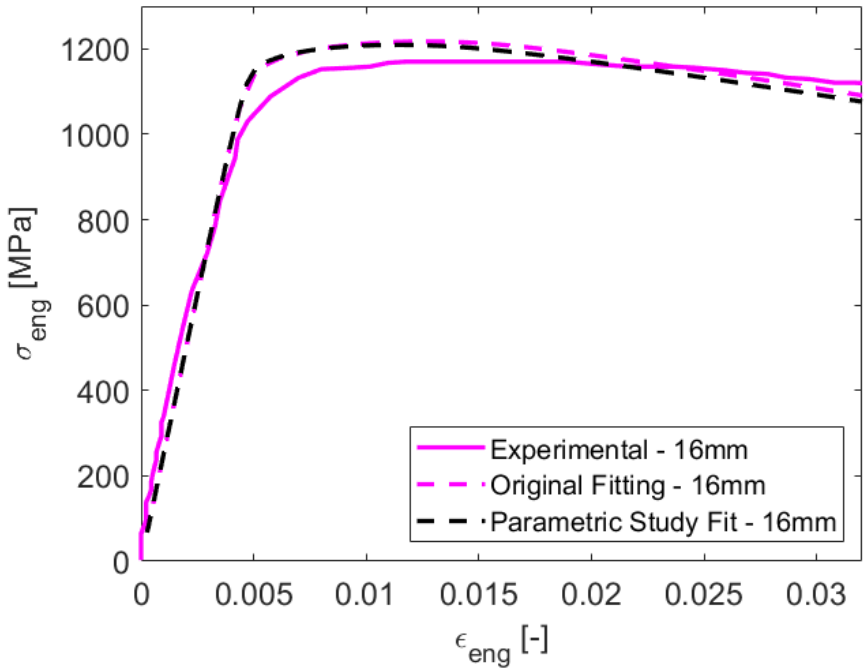

Figure 6.13: Validation parametric study for S960 steel

7

Results

This chapter shows the numerical and analytical results. The focus of this chapter is on plates with a 16 mm cutout, since the plate with a 8 mm cutout is prone to asymmetrical failure [13]. First, the influence of a finite width and length of the numerical model versus an infinite approach is discussed. Then, the results of the elasto-plastic behavior of the SCF including the elastic-perfectly plastic solutions are discussed. Next, the results of the transition of the elasto-plastic field across the width of the specimen are analyzed, including the numerical and analytical solution. Then, the calibrated material models of S690, S960, and S1100 are analyzed in terms of the behavior of the elastic/plastic SCF. Later, the numerical and analytical results of the local strain are considered. After this, the results of the parametric study are presented. Finally, a quantification of the main findings is given.

7.1. Infinite approach vs Finite

A theoretical value for the elastic SCF equal to 3 is obtained when an infinite width and length plate is simulated. The numerical model described in Chapter 5 uses a finite width and length based on actual specimen dimensions. When the stress concentration factor is plotted against the elongation at the gauge length, a stress concentration factor equal to 2.55 is obtained in the elastic portion. This is shown in Figure 7.1. The difference between this elastic SCF and the theoretical value can be explained by the influence of the finite width and length. The boundaries of the specimen have such an influence on the maximum stress that the elastic SCF does not reach the theoretical value. Section 5.2.2 explains the influence of the finite width and length in more detail. To simulate an infinite plate approach, the ligaments of the specimen are scaled by a factor of 6 resulting in a diameter/width ratio of 30. The SCF is shown in Figure 7.2. The SCF is determined by dividing the maximum stress at $r/a = 1$ and $\theta = \pi/2$, as described in Section 6.3. The gauge length elongation is determined by subtracting the displacements of the gauge length boundaries and dividing by the original gauge length.

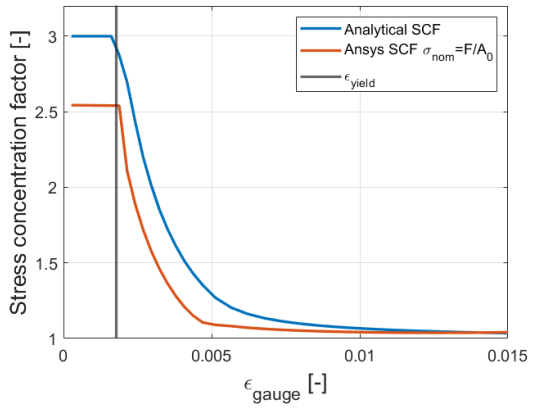

Figure 7.1: SCF as a function of elongation at gauge length finite approach

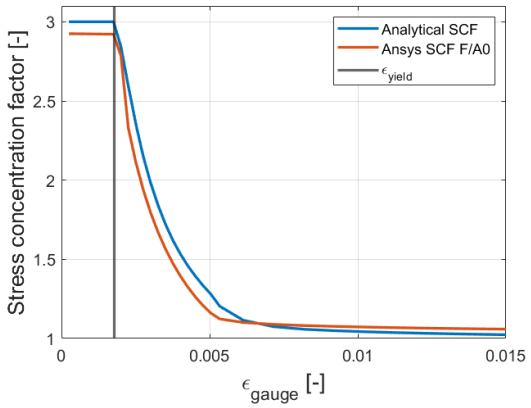

Figure 7.2: SCF as a function of elongation at gauge length infinite approach

7.2. Stress concentration factor

Figure 7.3 shows the results for the SCF versus normalized nominal stress. The nominal stress is divided by the yield stress to ensure a good comparison without the influence of the yield stress. The figure shows the results of the three different analytical methods previously discussed in Chapter 4, Stowell Applied, the Neuber method, and the Irwin method. An elastic-perfectly plastic solution is shown for the Neuber and Irwin methods. A solution for the Stowell Applied equation, which approximates an elastic-perfectly plastic solution, is also shown in the figure. In addition, the numerical results for an infinite plate approach are plotted in this figure. These numerical results show bumps which could be explained by time steps which are not small enough. Or, the plastic input in Ansys should be further discretized, i.e. smaller step sizes should be chosen.
This figure shows a good agreement between the analytical approximation methods and the calibrated numerical results. Also, the upper bound of the material is represented by the elastic-perfectly plastic solution. This solution is based on a strain hardening exponent equal or close to 1. All solutions give a linear solution for the elastic SCF , which is expected. Here, the boundary of the elastic part is indicated by the dashed grey line, which has a value equal to $\frac{\sigma_{ff}}{\sigma_y} = 0.33$. When yielding is initiated, the plastic SCF decreases.
The analytical results have a very good agreement with the values obtained by numerical simulation for the elastic-plastic behavior of the SCF. In conclusion, the analytical approaches of Stowell Applied and Neuber are validated.

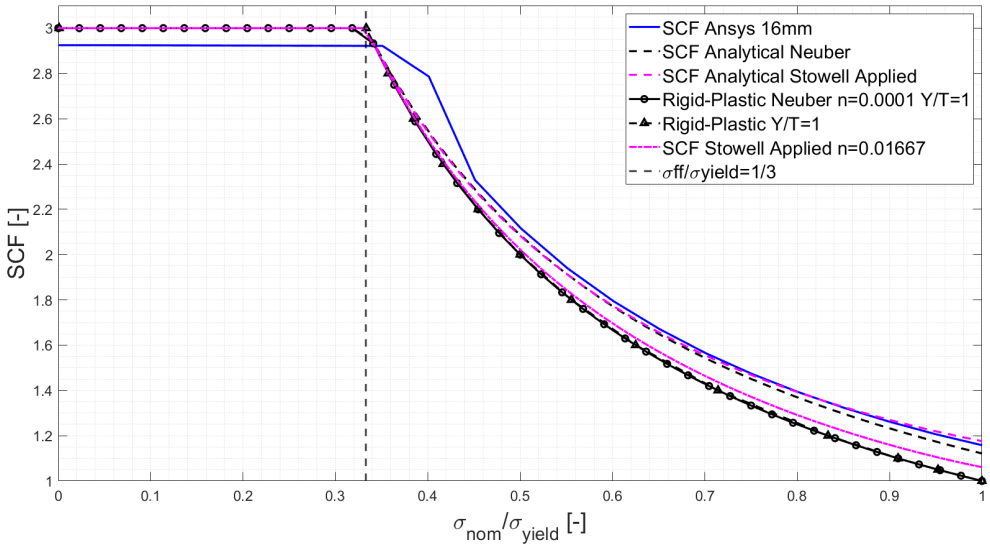

Figure 7.3: S960 SCF as a function of normalized nominal stress for an infinite plate

7.3. SCF versus r/a

The results related to the stress field are shown in this section. A numerical simulation of the calibrated material model of S960 steel is shown in Figure 7.4 and a schematic representation of the specimen including cutout is shown in Figure 2.5. The first figure shows the material behavior across the width of the material. The numerical simulation starts at r/a equal to 1, this is the edge of the circular cutout at $\theta = \frac{\pi}{2}$. An increasing r/a ratio means an increase perpendicularly across the width of the material to the edge with a constant value for θ. This figure clearly shows that for a $\frac{\sigma_{ff}}{\sigma_y}$ less than or equal to 0.33, which would be the theoretical point at which yielding would occur when the elastic SCF is equal to 3. The first three solutions overlap due to this elastic behavior. With a further increase of $\frac{\sigma_{ff}}{\sigma_y}$, the stress concentration factor also decreases due to the plastic behavior and the extent of the plastic zone also increases. At the point where the curve drops off again, the material behavior is elastic again.

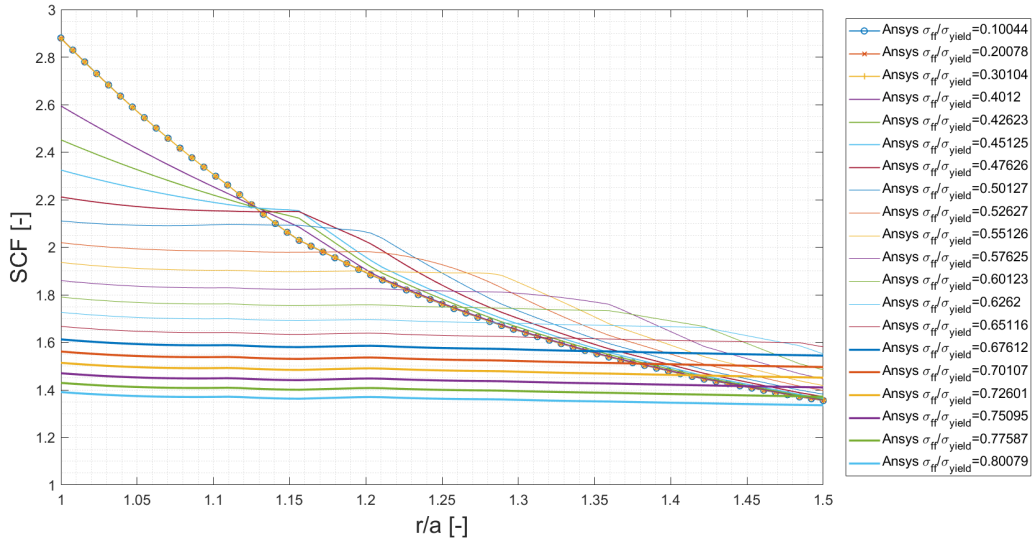

Figure 7.4: SCF as a function of r/a over the width of the S960 specimen for a 16 mm cutout

Besides the numerical simulation, a rigid analytical approximation via the Irwin analogy is also performed following the methodology described in Section 4.4. This method takes into account the extent in plastic zone as shown in the previous numerical simulation. The result is shown in Figure 7.5.
When strain hardening is considered and this is plotted against the rigid solution and the numerical solution for S960 steel, Figure 7.6 follows. This figure shows for higher values of normalized far field stress a better agreement compared to the numerical solution. The effect of hardening is shown in the analytical solution by the dashed lines, a slight decrease in plastic SCF across the width can be seen.

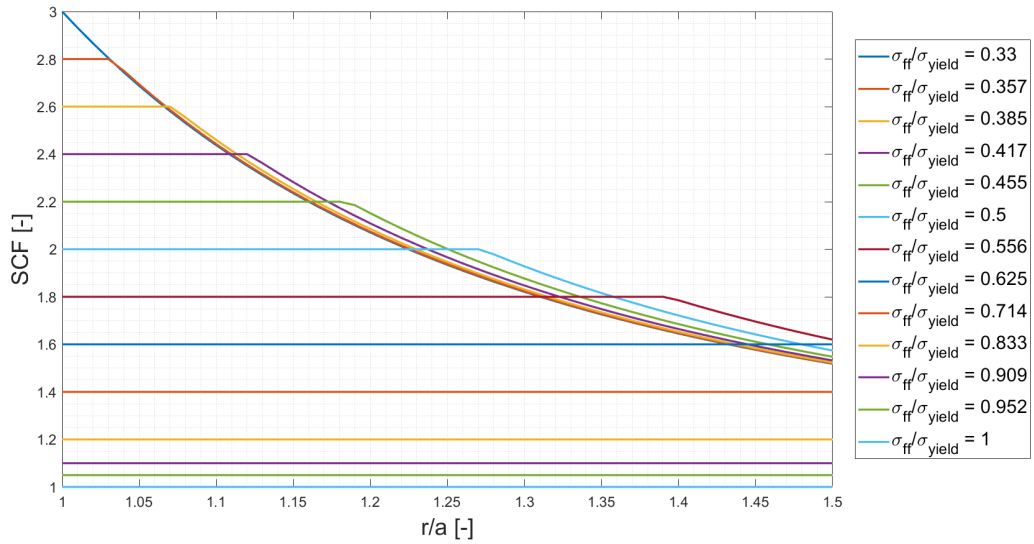

Figure 7.5: Elastic-perfectly plastic solution SCF as function of r/a - Irwin's method [41]

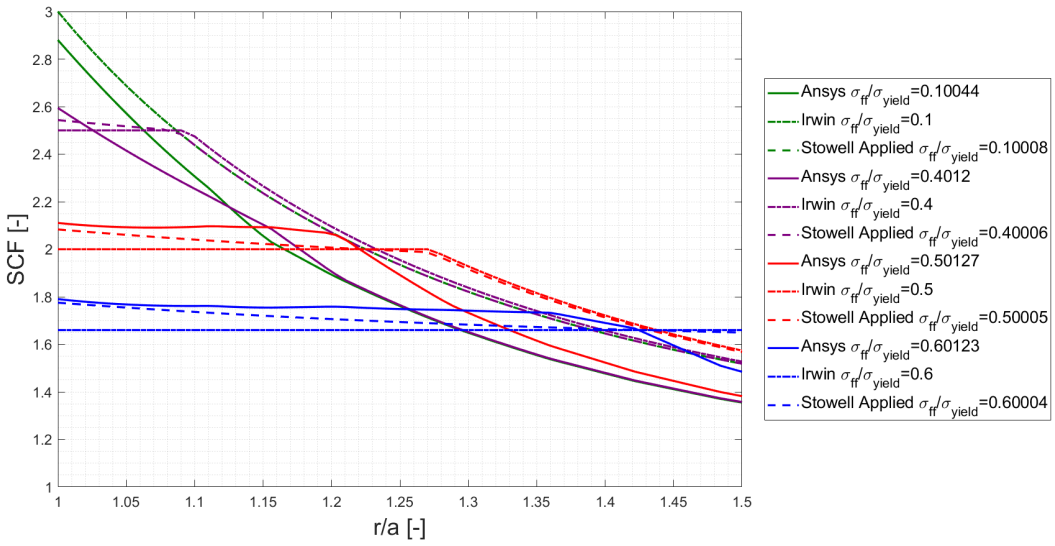

Figure 7.6: Analytical solution SCF over the width of the plate versus numerical solution

7.4. SCF around a circular cutout with different materials

Figure 7.7 shows the difference in stress field between the calibrated material models S690, S960 , and S1100 steel. The ratios $\frac{\sigma_{ff}}{\sigma_y}$ are chosen as close as possible to allow a fair comparison between the different materials. The blue and green curves, corresponding to S960 and S1100, each with a Y/T of 0.91, are very close or even overlap. If $\frac{\sigma_{ff}}{\sigma_y}$ were the same for both materials, the overlap would be even be more clear. Due to a remote displacement added to the numerical model instead of an added force, this ratio cannot be perfectly controlled with a limited number of time steps.
The figure also shows that the S690 material with a Y/T ratio equal to 0.955 has a lower plastic SCF for an almost identical $\frac{\sigma_{ff}}{\sigma_y}$. This could mean that the Y/T ratio has an impact on the SCF. This will be further investigated in the parametric study.

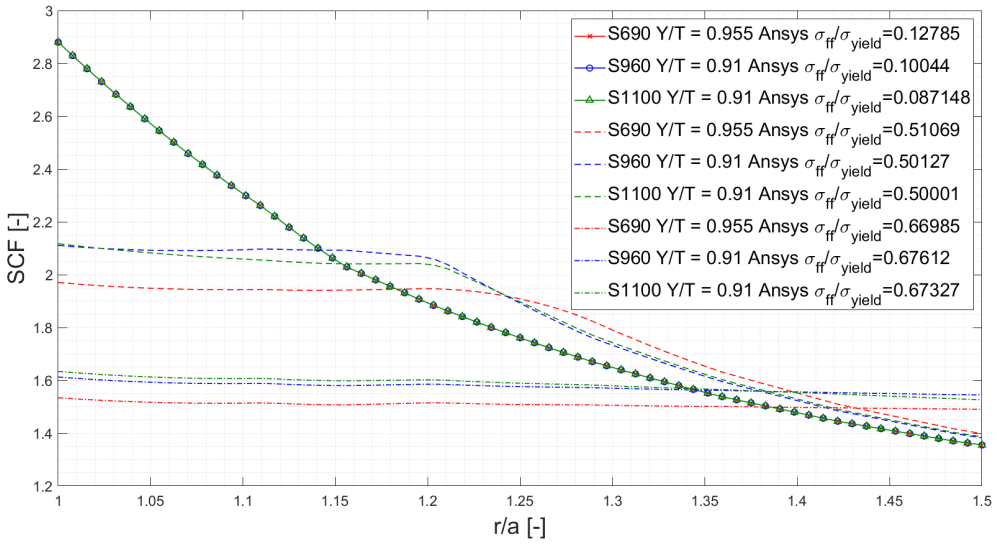

Figure 7.7: S690, S960 , and S1100 SCF as a function of the width of the specimen for $\sigma_{ff}/\sigma y \approx [0.1 \quad 0.5 \quad 0.67]$

Figure 7.8 shows for materials S690, S960, and S1100 the change in plastic SCF when r/a equals 1 and θ equals $\pi/2$. The observation made earlier that steel S690 has a lower plastic SCF than steels S960 and S1100 is further confirmed in this figure.

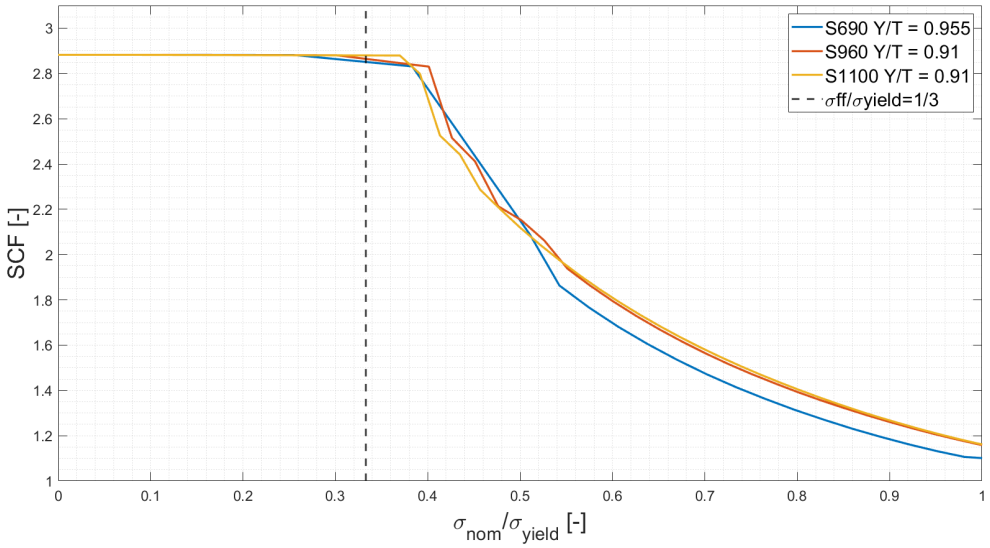

Figure 7.8: S690, S960 , and S1100 SCF as a function of dimensionless nominal stress for $\sigma_{ff}/\sigma y \approx [0.1 \quad 0.5 \quad 0.67]$ at $\theta = \pi/2$ and r/a=1

7.5. Local strain

It is essential to investigate the local strain if a conclusion is to be drawn about the structural integrity of the material, as strain is the governing parameter for ductile failure. In this section, the results of the analytical approach validated with the numerical data are presented. Section 7.6 discusses the results of the parametric study where the influence of four parameters is evaluated.

Figures 7.9 to 7.11 show the peak strain divided by the yield strain, the strain concentration factor, as a function of normalized nominal stress for materials S690, S960, and S1100. Using the term strain concentration factor is allowed when is assumed that the nominal strain is equal to the yield strain. The yield strain is calculated by dividing the yield stress by the Young's modulus. The analytical results of the Stowell Applied method and the Neuber method are also plotted in the same figures. A good approximation to the elasto-plastic behavior of the local strain is shown. Except for the yield plateau in the numerical results, this is not taken into account in the analytical solution. This causes a constant error that is larger for a larger yield plateau, but the trends of the behavior are similar and therefore useful. The error leads to a more conservative solution. The strain hardening exponent in the analytical solution for the Neuber approach is varied to show the expected behavior of the strain. Values close to zero, corresponding to high Y/T ratios, are chosen to see the influence of the hardening capacity of the material on the local strain. According to the analytical solution a decrease in the strain hardening exponent and thus an increase in the Y/T ratio leads to an increase in local strain. This is further investigated by numerical simulations in the parametric study in Section 7.6.

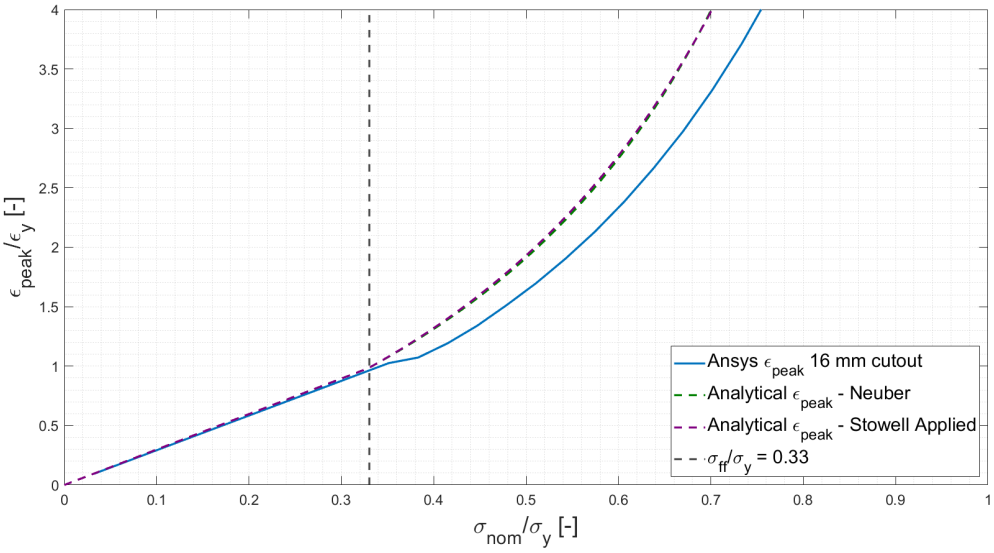

Figure 7.9: Analytical approximation local strain versus numerical results S690

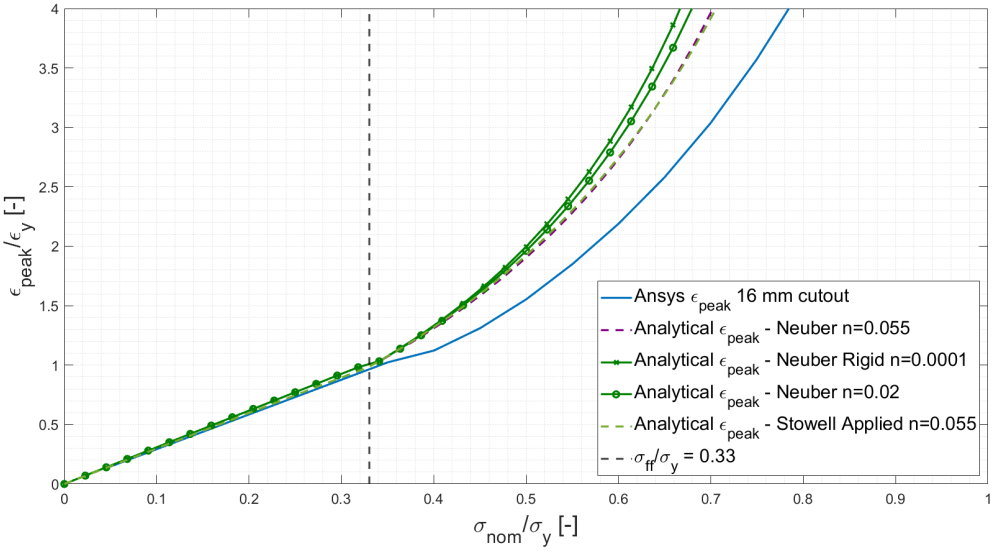

Figure 7.10: Analytical approximation local strain versus numerical results S960

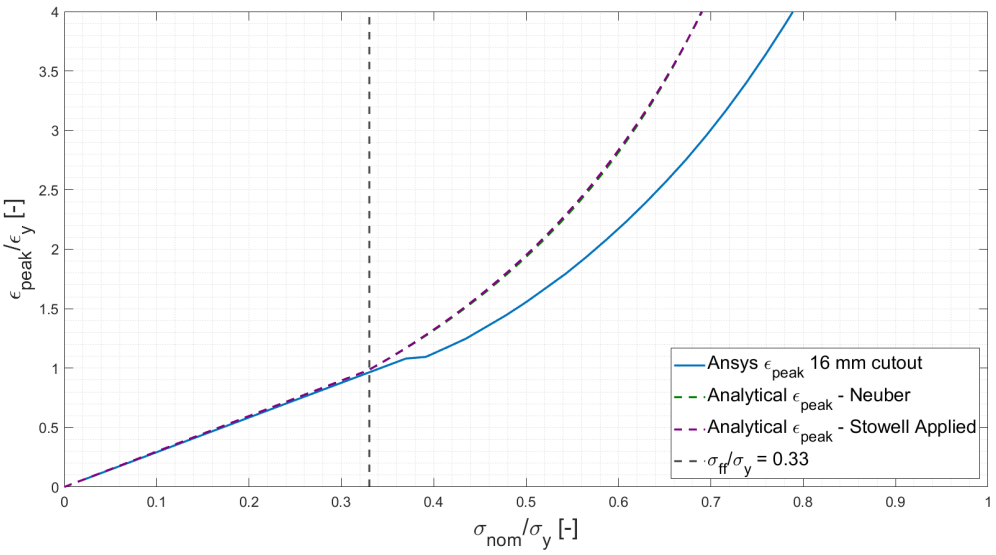

Figure 7.11: Analytical approximation local strain versus numerical results S1100

7.6. Parametric study

The analytical approach of the parametric study is described in Section 7.6. The results are divided into four subsections; varying Y/T, varying σ_y, varying n, and varying K. Each subsection consists of plots of SCF as a function of r/a , SCF versus the dimensionless nominal stress, and normalized ϵ_{peak} versus the normalized nominal stress. The yield strain, used for normalizing ϵ_{peak}, is calculated by dividing the yield stress by the Young's modulus. When Y/T is varied, the yield stress is kept constant and the tensile stress is varied. The same is true in reverse for the yield stress. When the strain hardening exponent n is varied, the strength coefficient K is kept constant. For the strength coefficient K, the same applies in the opposite direction.

7.6.1. Varying Y/T

Figure 7.12 shows the numerical results of SCF versus r/a for materials with a Y/T equal to 0.6, 0.86, 0.91, and 0.96. For all of these numerical models, three steps are plotted, with the normalized nominal stress being approximately 0.1, 0.45, and 0.67. For the first step, the material is fully elastic, so all three plots overlap. The second step results in a partially plastic field and a partially elastic field. The third step likewise, but with a larger extent of the plastic zone. In terms of the plastic SCF, when r/a equals 1, a small difference is observed between the four curves. The plastic SCF, which belongs to the lowest value of Y/T, has the highest value and the plastic SCF, which belongs to the highest value of Y/T, has the lowest value. Since the value for the normalized nominal stress is exactly the same due to conservation of energy, the areas below the curves for the different steps should be the same. This can be seen for the second step, where at r/a equal to 1 the plastic SCF is high, and after entering the elastic zone the plastic SCF is lowest compared to the other Y/T ratios. The extent of the plastic zone is not affected by the Y/T ratio. This is not clearly shown for the third step, since the r/a is limited to 1.5.

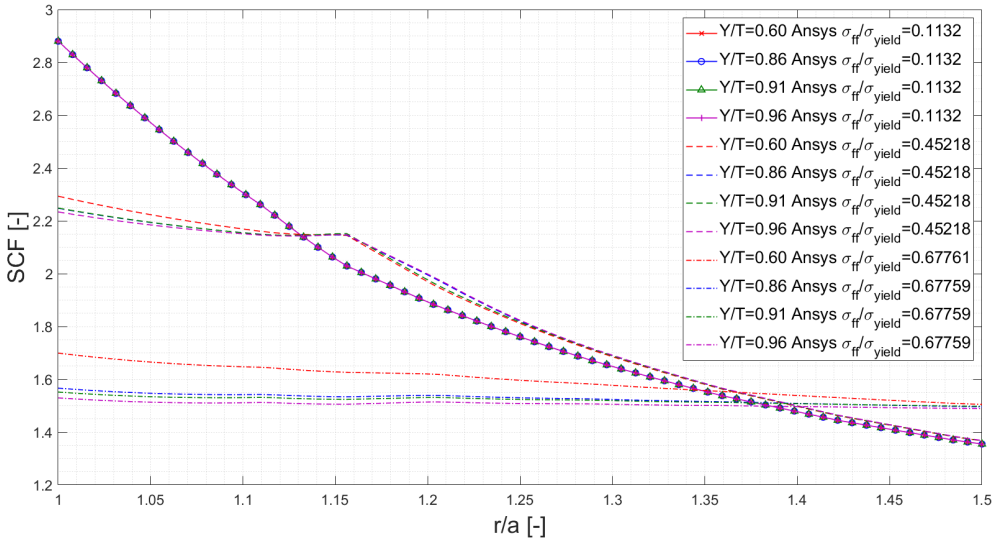

Figure 7.12: Influence Y/T on the stress field for Y/T = [0.6 0.86 0.91 0.96] and σ_y=976.25 [MPa]

The SCF as a function of the normalized nominal stress is shown in Figure 7.13 at location $\theta = \pi/2$ and r/a=1. The same observation is obtained as for the SCF versus r/a plot in terms of a decrease in plastic SCF for a higher Y/T ratio. This is also confirmed by the upper bound that follows from Neuber's analytical elastic-perfectly plastic solution.

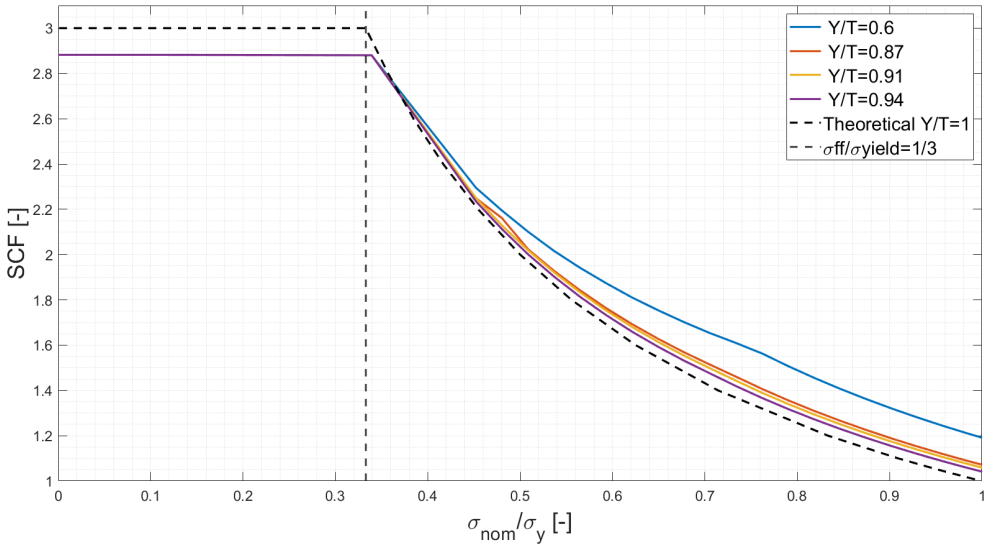

Figure 7.13: Influence Y/T on the SCF for Y/T = [0.6 0.86 0.91 0.96] and σ_y=976.25 [MPa] at $\theta = \pi/2$ and r/a=1

The influence of the Y/T ratio on the local strain can be assessed when the SCF is related to the local strain by Equation (4.25) in Section 4.5. Figure 7.14 shows the normalized peak strain versus the normalized nominal stress. This graph shows that an increase in Y/T leads to an increase in local strain. This has already been shown in an analytical manner in Figure 7.10. The graph with the analytical solution shows the relationship with a decreasing strain hardening exponent, which is closely related to an increasing Y/T.

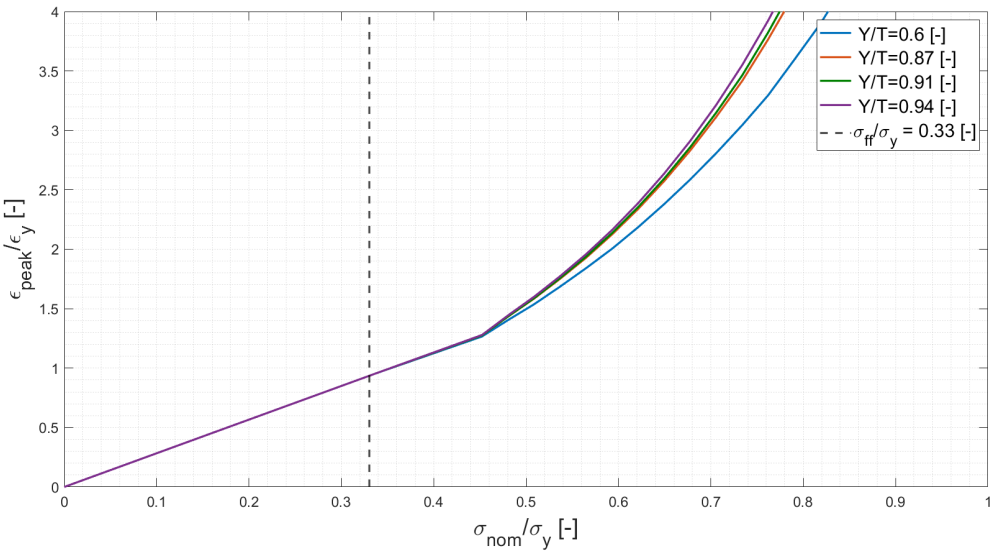

Figure 7.14: Influence Y/T ratio on local peak strain for Y/T = [0.6 0.86 0.91 0.96] and σ_y=976.25 [MPa] at $\theta = \pi/2$ and r/a=1

7.6.2. Varying yield stress

The second parameter that was varied in the parametric study is the yield stress. A yield stress equal to 690, 960, and 1100 [MPa] is evaluated with a constant value for the Y/T ratio equal to 0.95. Figure 7.15 shows the SCF as a function of r/a. Approximately the same normalized nominal stress values are used. However, due to the limited steps in the numerical simulation, the exact same values could not be chosen. In the figure shown, this leads to a distorted representation since the curves for each normalized nominal step should overlap. This can be confirmed by considering a normalized nominal stress value corresponding to about 0.5. The curve representing a yield stress equal to 690 has a value less than 0.5 and is therefore at an "earlier" step of the graph. To confirm this explanation, Figure 7.16 shows the SCF versus normalized nominal stress. This figure shows that the curves overlap, confirming the previous explanation. Both figures imply the same observation that the yield stress has no effect on the stress concentration factor.

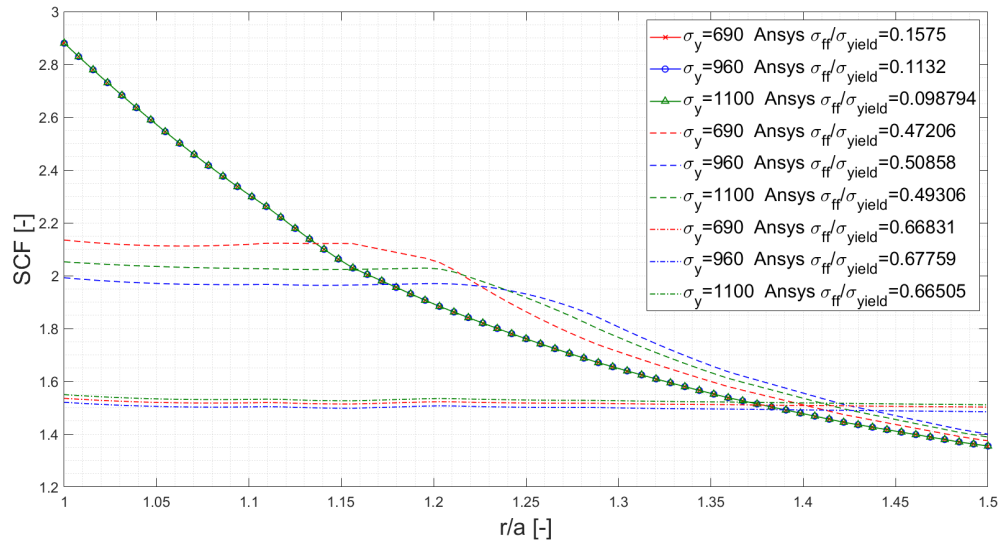

Figure 7.15: Influence σ_y on the stress field for nominal yield strengths of 690, 960, and 1100 [MPa] with Y/T=0.95

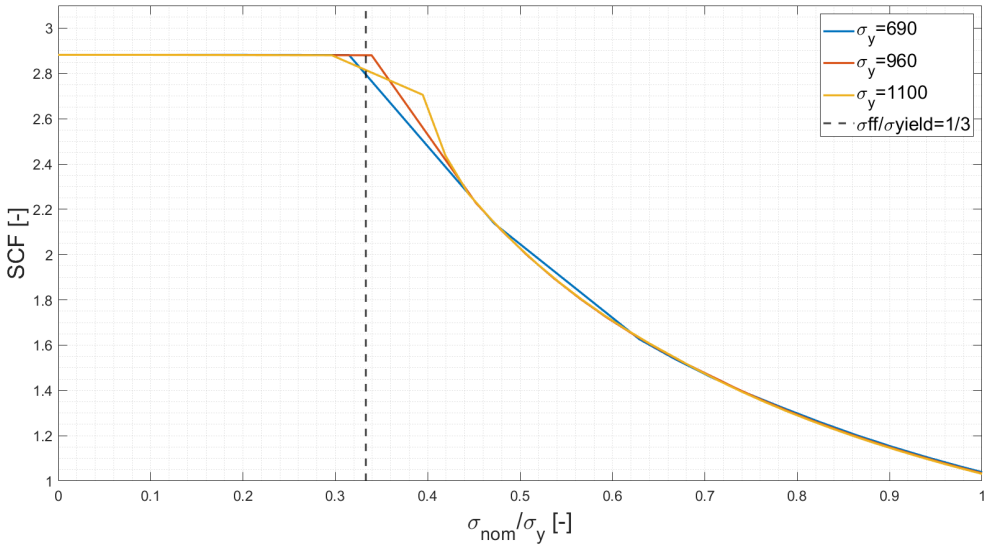

Figure 7.16: Influence σ_y on the SCF for σ_y = [690 960 1100] [MPa] and Y/T=0.95 at $\theta = \pi/2$ and r/a=1

Relating the SCF back to the local strain using Equation (4.25) yields Figure 7.17. From this figure, it can be seen that the normalized local strain is not affected by a change in yield stress when the curves are normalized by dividing by the yield stress.

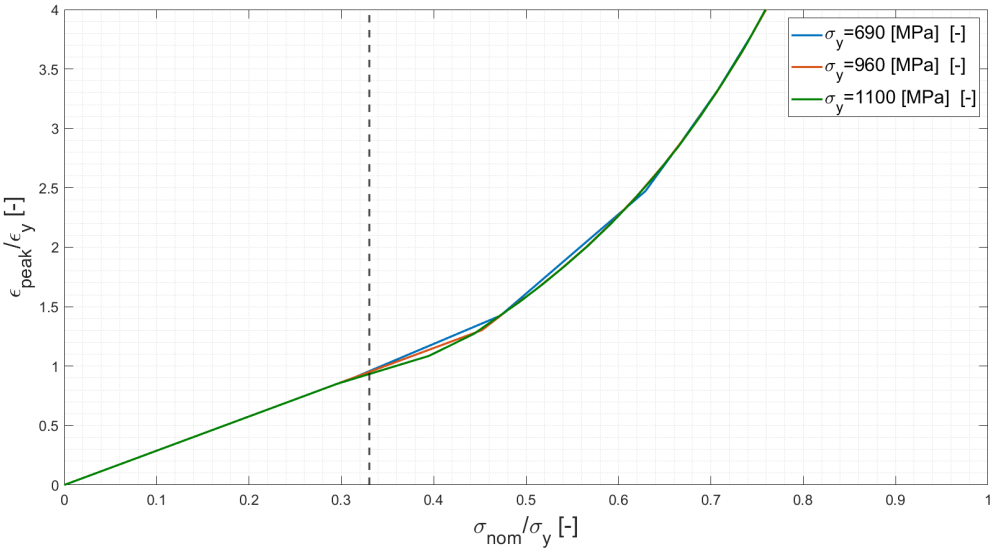

Figure 7.17: Influence σ_y on the local peak strain for σ_y = [690 960 1100] [MPa] and Y/T=0.95 at $\theta = \pi/2$ and r/a=1

7.6.3. Varying strain hardening parameter

The third parameter changed is the strain hardening exponent n while the strength coefficient K remains constant. For n, a value equal to 0.0001, 0.02, 0.0282, 0.04, .05, and 0.06 is used. The value of 0.0282 is the original value which belongs to the yield stress of 960 [MPa]. Figure 7.18 shows the effect of varying this parameter on the stress field. It is not possible to obtain definite relationships from this figure as the normalized nominal stress is not perfectly equal and therefore it is difficult to extract relationships with this amount of data. Therefore, Figure 7.22 provided a better insight since the nominal stress is normalized. This figure shows that the differences are small, but there is a slight effect of the strain hardening parameter on the plastic SCF. A decrease in the strain hardening exponent leads to a decrease in plastic SCF. This is consistent with the results from varying the Y/T ratio, as a

higher Y/T ratio is related to a low value for n .

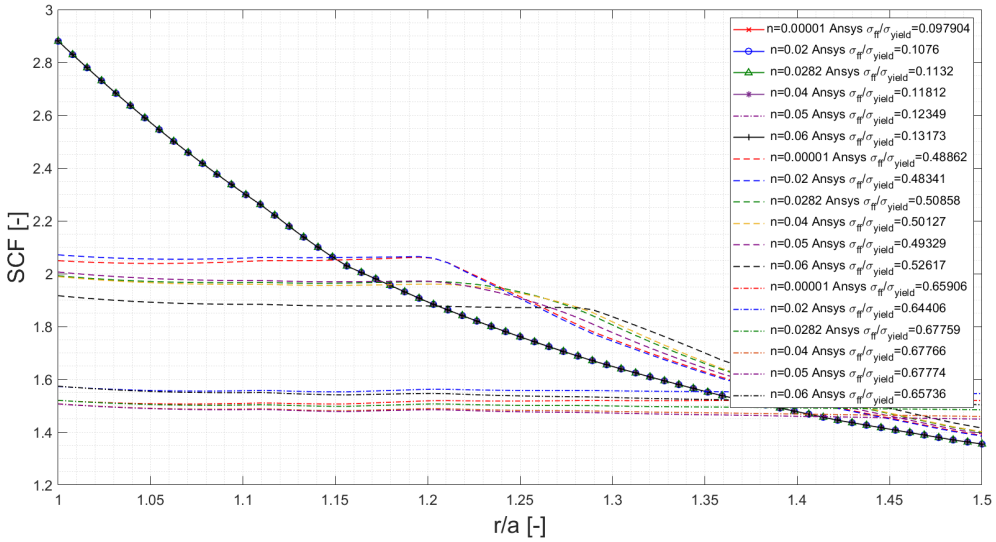

Figure 7.18: Influence n on the stress field for n = [0.00001 0.02 0.0282 0.04 0.05 0.06] and K=1117

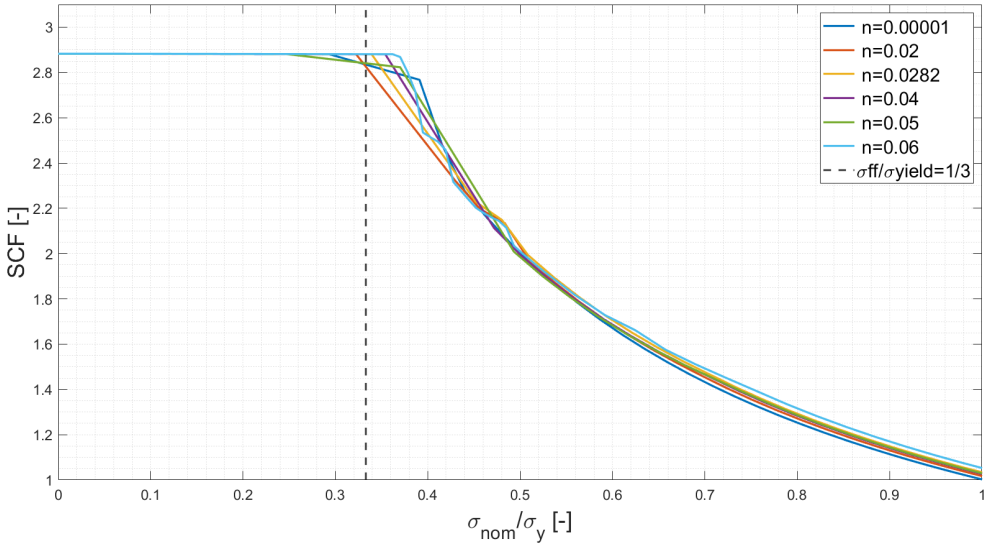

Figure 7.19: Influence n on the SCF for n = [0.00001 0.02 0.0282 0.04 0.05 0.06] K=1117 at $\theta = \pi/2$ and r/a=1

Relating the SCF to the local epsilon again with Equation (4.25) results in Figure 7.20. This figure shows that a decrease in the strain hardening parameter leads to an increase in the local strain. This is also consistent with the results from the varying Y/T ratio, as a higher Y/T ratio is associated with a lower value of the strain hardening exponent n. As a result of linear interpolation between a limited numbers of data points, a distorted picture of reality is shown in the range of normalized nominal stress between 0.3 and 0.4. The curves should all be constant up to a normalized nominal stress equal to 0.33 as this is the theoretical elasticity limit.

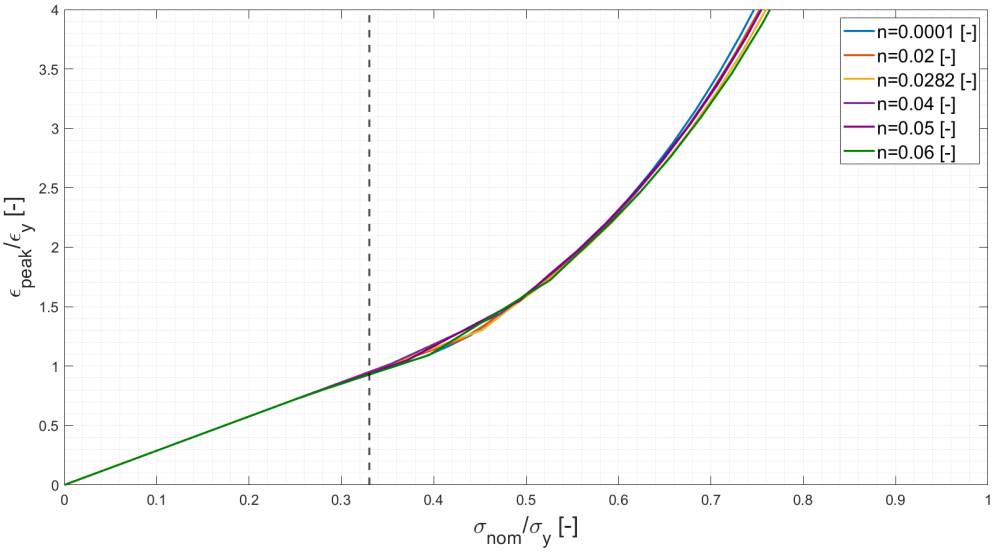

Figure 7.20: Influence n on the local strain for n = [0.00001 0.02 0.0282 0.04 0.05 0.06] K=1117 at $\theta = \pi/2$ and r/a=1

7.6.4. Varying K

The fourth and final varied parameter varied is the strength coefficient K. While K is varied, the strain hardening exponent remains constant. Figure 7.21 shows the SCF as a function of r/a for a varying value of the strength coefficient. Slight differences in behavior are observed, which may be related to the slight differences in the normalized nominal stress. This is also confirmed by Figure 7.22, where the nominal stress is normalized on the x-axis. Both figures show that the strength parameter has no effect on the SCF.

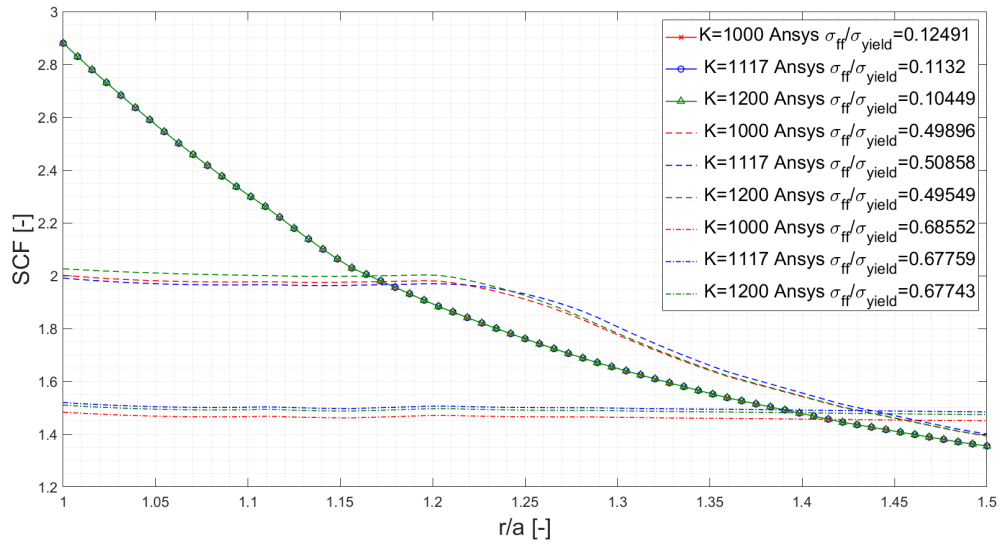

Figure 7.21: Influence K on the stress field for K = [1000 1117 1200] and n=0.0282

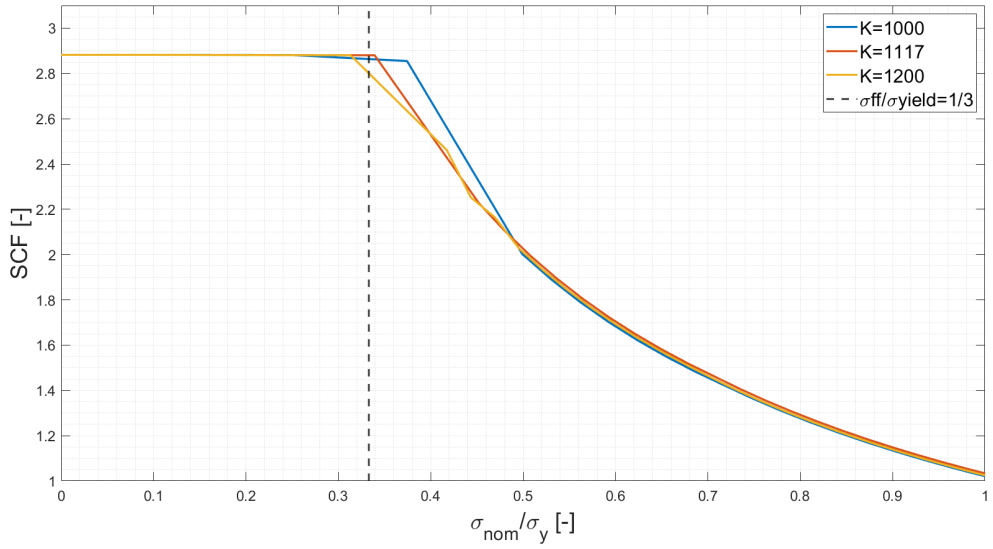

Figure 7.22: Influence K on the SCF for K = [1000 1117 1200] and n=0.0282 at $\theta = \pi/2$ and r/a=1

Focusing on the local strain by using Equation (4.25) to relate the SCF to the local strain leads to Figure 7.23. This figure shows that the strength coefficient has no effect on the local strain.

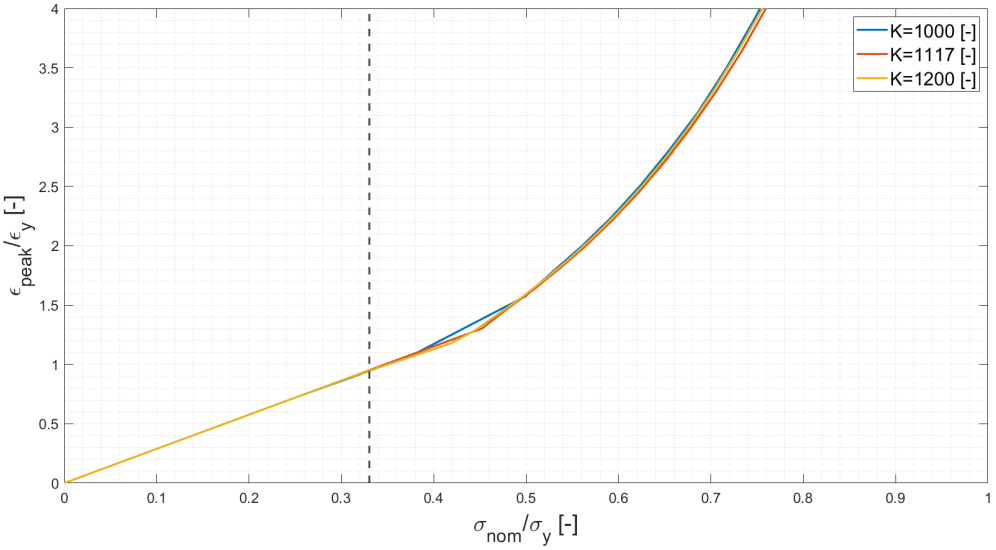

Figure 7.23: Influence K on the local strain for K = [1000 1117 1200] and n=0.0282 at $\theta = \pi/2$ and r/a=1

7.7. Quantification

The quantification of the results is useful to see the real influence of certain parameters and to answer more precisely the main question about the influence of the Y/T ratio on the stress field. The collected results are selected at interesting values in the plots. The values are noted at a normalized nominal stress of 0.67, which is 2/3 of the yield stress. This value was chosen because this is the design limit for Huisman Equipment set by classification societies with which Huisman Equipment works: Lloyds, DNV-GL, and Bureau Veritas [19, 33, 39]. The results of the parametric study are used for quantification as these provide the most consistent findings on the effects of the parameters. Since the parameters Y/T and the strain hardening exponent are the only parameters that tend to have an impact, this is further quantified with $\frac{\sigma_{nom}}{\sigma_y} = 0.67$.

Table 7.1 and 7.2 show the results for the SCF and normalized local strain. Due to an applied far-field displacement in the numerical model combined with limited time steps, the values for the plastic SCF and the local strain are to be interpolated according to the normalized nominal stress equal to 0.67. These tables show that a 2.4% decrease of plastic SCF occurs for the Y/T between 0.94 and 0.87. Between 0.6 and 0.87, the decrease from plastic SCF is equal to 8.48%. For normalized local strain, these values correspond to an increase of 9.4% and 2.8%, respectively. Thus, an increase in Y/T causes a slight decrease in plastic SCF and a slight increase in local strain.
Varying the strain hardening exponent results in even smaller percentages. A value for n equal to 0.02 compared to an n equal to 0.06 leads to an increase in plastic SCF equal to 1.87% and an n close to zero compared to an n equal to 0.02 results in an increase in plastic SCF equal to 3.30%. The normalized local strain percentages are equal to 1.04% and 6.2%, respectively. Thus, the strain hardening parameter also has a small effect on the plastic SCF and strain hardening exponent. According to Leis, the used strain hardening exponents correspond to Y/T ratios equal to 1, 0.97, 0.95, 0.917, 0.887, and 0.857 for n values equal to 0.00001, 0.02, 0.0282, 0.04, 0.05, and 0.06, respectively.

Table 7.1: Quantifying parametric study - Y/T ratio

Y/T	0.6	0.87	0.91	0.94
SCF	1.701	1.568	1.553	1.531
$\epsilon_{peak}/\epsilon_y$	2.586	2.83	2.858	2.91

Table 7.2: Quantifying parametric study - strain hardening exponent

n	0.00001	0.02	0.0282	0.04	0.05	0.06
Y/T	1	0.97	0.95	0.917	0.887	0.857
SCF	1.467	1.5145	1.5216	1.5247	1.5242	1.5429
$\epsilon_{peak}/\epsilon_y$	3.1514	2.9667	2.946	2.955	2.963	2.936

8

Conclusion

The study can be roughly divided into five parts, into which the conclusion will also be divided. The literature review, the analytical models, the FEA models in Ansys, the validation, the results, and the quantification of the results.

The aim of the literature review was to identify the research gap. The research gap that was found in the literature review is the missing analytical relationship between the Y/T ratio and stress fields for high strength steels. Therefore, the research question reformulates this research gap with the aim of answering this question.

In the analytical study, a mathematical relationship between the the Y/T ratio and the strain hardening exponent is found. Moreover, the methods Stowell Applied and Neuber are validated with numerical data. The Stowell Applied method is developed in this research and is based on the Stowell equation. In the analytical part, a method for the stress field based on the Irwin analogy is given, and an analytical formulation for the local strain based on Stowell's approach is established. At the end of the analytical part, the parametric study is described using the yield strength and Y/T ratio as input. This input is used to find the strain hardening parameter and the strength coefficient using the described equations, which are used in combination with Hollomon's law as a plastic input for a material model in Ansys.
The parametric study includes variation of Y/T ratio, yield strength, strain hardening parameter, and strength coefficient. A method is formulated using experimental data from Bannister in combination with basic stress-strain relationships [2]. This method provides a wide range of possible combinations of material properties.

For the numerical part, numerical models are created and calibrated in Ansys with FEA and used at the end to validate the analytical equations. In terms of calibration, the material models of Stofregen and VTT are calibrated by simulating a standard tensile test with a material model by FEA in Ansys using Hollomon's law. It is also found that a model in FEA in Ansys is able to simulate a standard experimental tensile test correctly. This answers the sub-question of the research question on how to describe the hardening behavior of high strength steels in the best way. Using the calibrated numerical material models, the analytical models are also validated. Furthermore, it is concluded that the parametric study is validated by simulating the material properties of S960 steel and comparing the stress-strain curves resulting from the parametric study method and the calibrated material model.

The results of the numerical and analytical models are presented in Chapter 7. With respect to the numerical models, with the original specimen and the ligaments of the specimen scaled by a factor of 6, it can be seen that the influence of the edge is significant. Scaling the specimen by a factor of 6 gives a good representation of an infinite length and width. Therefore, a scaled specimen should be used in further comparisons with the analytical results as they are based on an infinite plate type.
It can also be noted that the elastic SCF is constant when the material behaves elastically, and decreases as it enters the plastic zone. This can be properly described by the analytical methods Stowell Applied and Neuber. The rigid-plastic solutions of Irwin and Neuber show a lower bound of the plastic SCF when no hardening occurs. A near-zero solution of Stowell Applied shows the same trend.

The lower bound, which is zero hardening, is useful because this is the worst case scenario. As the material enters the plastic zone, the plastic SCF decreases due to the redistribution of energy. This decrease causes a reduction in stress peaks and is therefore important for engineering practise. The sub-question about the analytical description of the stress field can be partially answered with this information at the edge of the circular cutout.
Looking at the results for the SCF as a function of specimen width, it can be seen that the extent of the plastic zone increases with normalized nominal stress. An analytical rigid solution based on Irwin's approach yields a stress field with a similar change in the extent of the plastic zone. Comparison of the rigid analytical solution, the analytical solution that includes strain hardening and is based on the method Stowell Applied, and the numerical solution, gives a relatively good fit for the rigid plastic solution. The solution that includes strain hardening does not (yet) account for the change in the extent of the plastic zone. The sub-question of the research question concerning the analytical description of the stress field can be answered. This can be described by a rigid solution in analogy to the Irwin method. Also the Stowell Applied describes the stress field in a suitable way including the shift in plastic zone.
When material models for common steels S690, S960, and S1100 are compared in terms of SCF with the width of the specimen and the normalized nominal stress, a conclusion is drawn. An increase in the Y/T ratio leads to a decrease in plastic SCF. These material models are also compared separately with the analytical solution of Stowell Applied and Neuber for the local strain. It is concluded that the yield plateau, shown in the plots for local elongation, is not included in the analytical solution. Nevertheless, the analytical solutions are a good approximation to the numerical results. It can also be concluded from the increase in the strain hardening parameter in the approach Neuber Derived for S960 that this leads to an increase in the local strain.

Looking at the results of the parametric study, an increase in Y/T ratio leads to a decrease in plastic SCF. The extension of the plastic zone does not change under the influence of a changing Y/T ratio. An increase in Y/T ratio leads to an increase in the local strain.
Varying the yield strength has no effect on the extent of the plastic zone and plastic SCF. It also has no effect on the local strain.

From the variation of the strain hardening exponent, it is concluded that a decrease leads to a slight decrease in plastic SCF. Looking at the local strain, it is concluded that a decrease in the strain hardening exponent leads to an increase in local strain. These relationships are to be expected since the strain hardening exponent is closely related to the Y/T ratio via the Leis equation.
The last varied parameter in the parametric study is the strength coefficient. It is concluded that the variation of this parameter has no effect on the stress field or SCF. Also, the variation of the strength coefficient has no effect on the local strain.

When the influencing parameters are quantified at $\frac{\sigma_{ff}}{\sigma_y} = 0.67$, it can be seen that a change in Y/T from 0.6 to 0.87 results in an 8.48% decrease in plastic SCF and a 9.4% increase in local strain. Between a Y/T of 0.87 and 0.94, a decrease of 2.4% in plastic SCF and an increase of 2.8% in local strain is observed. Increasing the strain hardening exponent from 0.00001 to 0.02 results in a 3.3% increase in plastic SCF and a 6.2% decrease in local strain for $\frac{\sigma_{ff}}{\sigma_y} = 0.67$. Increasing the strain hardening exponent from 0.02 to 0.06 results in a 1.87% increase in plastic SCF and a 1.04% decrease in local strain at the same normalized nominal stress.

Ultimately, the research question “What is the influence of the yield to tensile strength ratio on the stress fields of highs strength steels?” can be answered with additional information. An increase in the Y/T ratio results in a relatively small decrease in the plastic SCF. A change in the Y/T ratio has no effect on the extent of the plastic zone. Thus, the Y/T ratio has an effect on the plastic SCF of the specimen. The parametric study shows that increasing the Y/T ratio leads to an increase in local strain. The parametric study also shows that in addition to the Y/T ratio, the strain hardening exponent also has an effect on the plastic SCF and the local strain. According to this study, the yield stress, and the strength coefficient have no influence on the SCF and the local strain.

9

Discussion and recommendation

First, this chapter will provide an interpretation of the results. Then, this chapter will discuss the relevance of the research. After that, the limitations of the research will be discussed. In the end, recommendations for future research will be provided.

9.1. Interpretation

The first results presented show that the numerical material models of S690, S960, and S1100 materials are calibrated with the actual experimental data of standard tensile tests. This means that the numerical models show the same behavior as the specimen in an experiment. The same is true for the analytical methods such as Stowell Original, Stowell Applied and the Neuber method. These methods are also validated and thus realistically represent the actual material behavior.
The described behavior of the SCF in Figure 7.3, a decreasing plastic SCF with increasing normalized nominal stress, can be explained. The SCF is constant in the elastic zone and the SCF decreases when entering the plastic zone. This means that the material redistributes energy by extending the plastic zone, resulting in a decrease in plastic SCF. If the material has strain hardening capacity, i.e., a Y/T ratio less than 1, the decrease in plastic SCF is slower. As the analytical equation and results show, the local strain can be related to the SCF. The relationship shows that the local strain increases when the plastic SCF decreases. This can be explained by the fact that a decrease in plastic SCF is associated with an increase in the size of the plastic zone due to energy redistribution. When the plastic zone is increased, the elongation also increases, resulting in a larger local strain.
The analytical results versus the numerical results of the local strain show a systematic mismatch. There seems to be a yield plateau that is not accounted for in the analytical method. However, the analytical methods are still very useful as they still describe the correct trend, which is linear in the elastic part and increasing in the plastic part for increasing normalized nominal stress.
The influence of the Y/T ratio on the plastic SCF and on the local strain also give good insights. An increasing Y/T ratio leads to a decrease in plastic SCF and an increase in local strain. This means that a material with a higher Y/T ratio tends to have a higher strain distribution compared to a material with a lower Y/T ratio.

9.2. Relevance

Investigating the influence of parameters such as the Y/T ratio on the behavior of high strength steels is extremely relevant. As structures tend to get larger and are built for higher capacities, the structure needs to be stronger. Therefore, higher strength steels play a very important role. Identifying the influence of parameters such as the Y/T ratio on the behavior of high strength steels potentially provides an opportunity to test established design criteria. In the end, if it can be shown that an increase in the Y/T ratio leads to a small reduction in the failure load, this could lead to a flexibilisation of the rules. Stress concentrations play a very large role in the potential failure of structures. A stress concentration can lead to local strain, which can lead to local fracture and eventually global fracture. Local strain directly leads to possible local fracture as this is the governing factor for ductile failure.

The analytical formulations are also very useful. They are simple and generally applicable. So they can be used for quick hand calculations in a very efficient and valid way. The parametric study uses the analytical formulas in combination with Bannister's experimental data [2]. This is also very relevant because the described method can be used to artificially generate a wide range of material properties and implement them in a FEA model in Ansys. In this way, experimental data from standard tensile tests are not required and engineers can easily generate elasto-plastic models in Ansys to check the influence of changed material properties on stress fields.

9.3. Limitations

A limiting factor in this research was computational time. In this research, it was concluded that the ligaments of the geometries of the FEA models in Ansys should be scaled by a factor of 6 to get rid of the influence of the boundaries on the behavior. This resulted in a dramatic increase in computation time. This approach also likely resulted in "bumpy" plots. These could possibly be refined if the number of time steps could be increased.
Another limiting factor is that only ductile failure is considered in his study. The Y/T ratio could have a different influence on other failure modes, which could be interesting as other modes also occur in real situations.
In addition, the lack of a failure criterion in the numerical model is a limitation. At the beginning of the research it was chosen that no failure criteria will be formulated as this would be too much work for a nine month research. However, this could give engineers more concrete insight into the actual effects of an increasing Y/T ratio to consider in their designs.
Also, a limiting factor is considering only a circular cutout as a discontinuity. The last identified limitation of this research is the assumption of infinitely large ligaments of the specimens.

9.4. Recommendations

A failure criterion for ductile failure should be implemented in the numerical model in a future research. This will help to achieve the global goal of determining the influence of the Y/T ratio on the failure load of high strength steels. This will yield the influence of strain hardening capacity on the actual failure load.
To further optimize the results generated in this study for the infinite models in Ansys, smaller time steps could be chosen to produce a smoother curve. Also, further discretization of the plastic input into the multi-linear isotropic hardening could be achieved. More, and smaller steps should be chosen for the plastic strain input.
In further research, the Neuber approach could be applied to other types of discontinuities. In this research, the approach is used only for circular cutouts with a theoretical elastic SCF equal to 3. The equation could be updated for a discontinuity with a different theoretical elastic SCF and replace the factor 3 in Neuber's equation.
Moreover, in this study, the SCF is solved numerically for the Stowell Applied method. Efforts could be made to find an algebraic expression that can be solved by a simple hand calculation. This would benefit the applicability of this method, because at the moment a numerical solver is needed.

A

Experimental Results Standard Tensile Tests Stofregen and VTT

This appendix shows the experimental results of the standard tensile tests performed by Stofregen [35] and VTT [12]. Figure A.1 shows the results for plain steel specimen of grades S690 and S1100, respectively. The figure shows that the higher grade has a significantly higher yield strength.

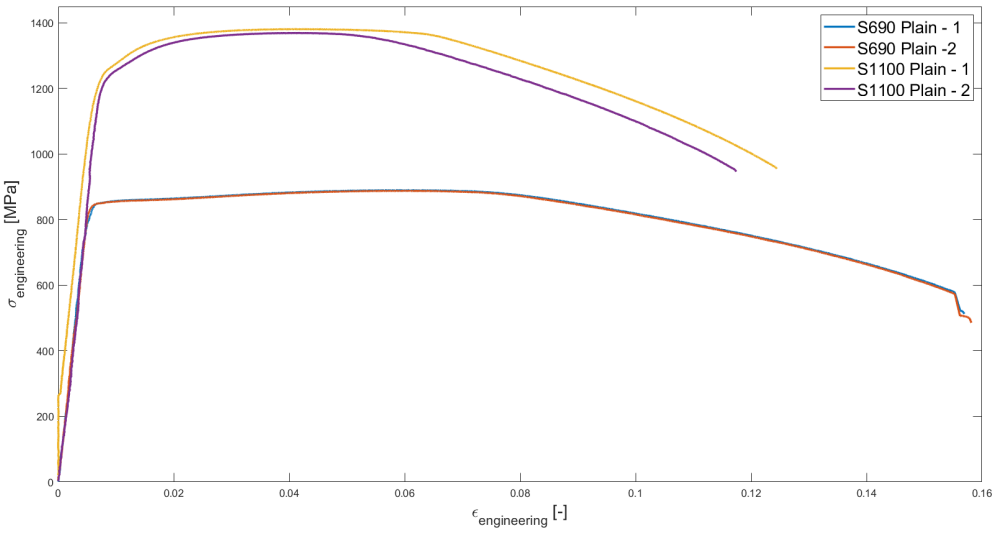

Figure A.1: S690 and S1100 - Standard Tensile Test Results Stofregen Plain Steel

Figure A.2 shows the results for steel specimens with a notch of 2mm of grades S690 and S1100, respectively. The figure shows that the failure strain is reached earlier. The value for the ultimate tensile strength is also higher for a specimen with a notch compared to plain steel. This can be explained by the presence of a SCF.

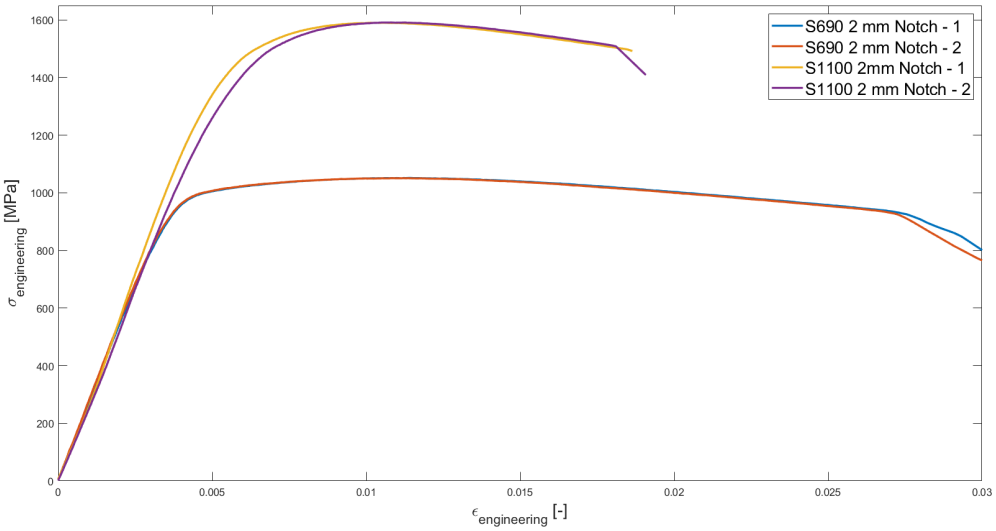

Figure A.2: S690 and S1100 - Standard Tensile Test Results Stofregen 2 mm Notch

Figure A.3 shows the results for steel specimens with a notch of 4mm of grades S690 and S1100, respectively. The figure shows that the failure strain is achieved in a later stage compared to the 2 mm notch. Moreover, the value for the ultimate tensile strength is higher for a specimen with a notch compared to plain steel. This can be explained by the presence of a SCF.

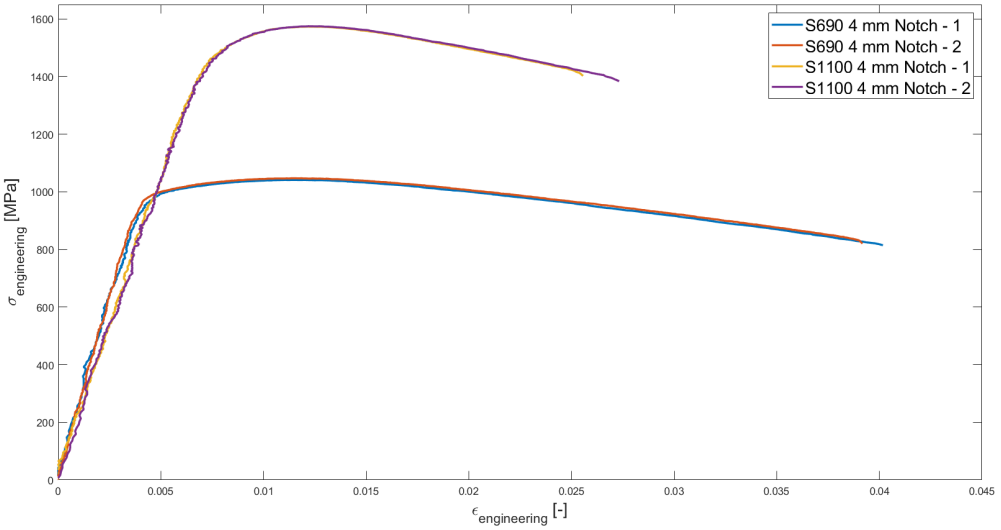

Figure A.3: S690 and S1100 - Standard Tensile Test Results Stofregen 4 mm Notch

Figure A.4 shows the standard tensile test results of VTT using specimens with a circular cutout varying from 0 to 40 mm. A larger diameter for the cutout tends to result in a larger ultimate stress compared to lower values for the diameter.

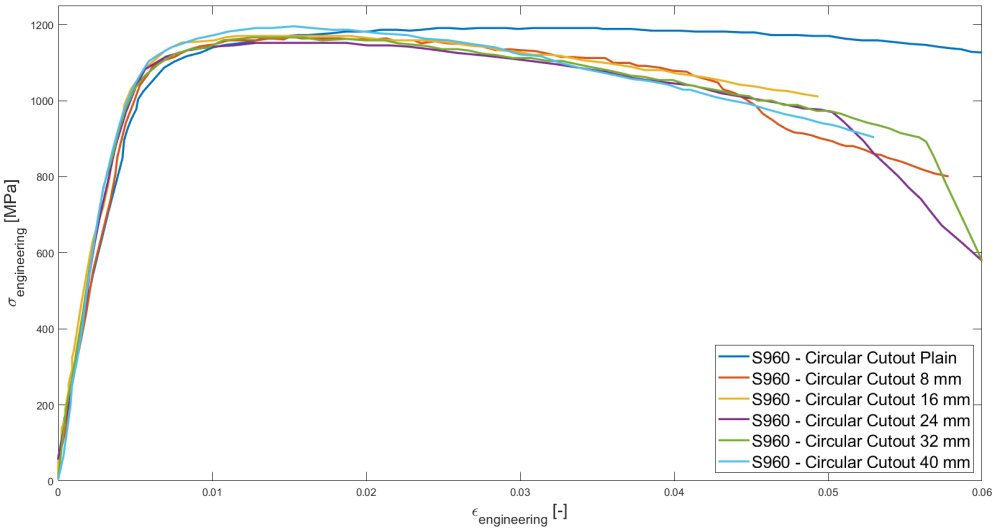

Figure A.4: S960 - Standard Tensile Test Results VTT Varying Circular Cutout

B

Design cases

Besides interest in academic results, Huisman Equipment is also interested into actual design cases. These cases will be useful for engineers of Huisman Equipment to see the influence of changing the material properties yield and tensile strength. Three cases will be looked into with respect to elasto-plastic SCF and local strain. These parameters will be calculated analytically and numerically.

Cases shown in Table B.1 are looked into. Case I is the benchmark case fulfilling the minimal design requirements of Huisman Equipment. Figure B.1 shows the results for the elasto-plastic SCF as function of the normalized nominal stress. As shown in this figure, the plastic SCF is lower for materials with a higher Y/T ratio as expected. Figure B.2 shows the normalized local strain as function of the normalized nominal stress. This figure shows that a higher Y/T ratio results in a higher local peak strain.

Table B.1: Design cases

	σ_y [MPa]	σ_{UTS} [MPa]	Y/T [-]
Case I	690	770	0.896
Case II	760	770	0.987
Case III	690	700	0.986

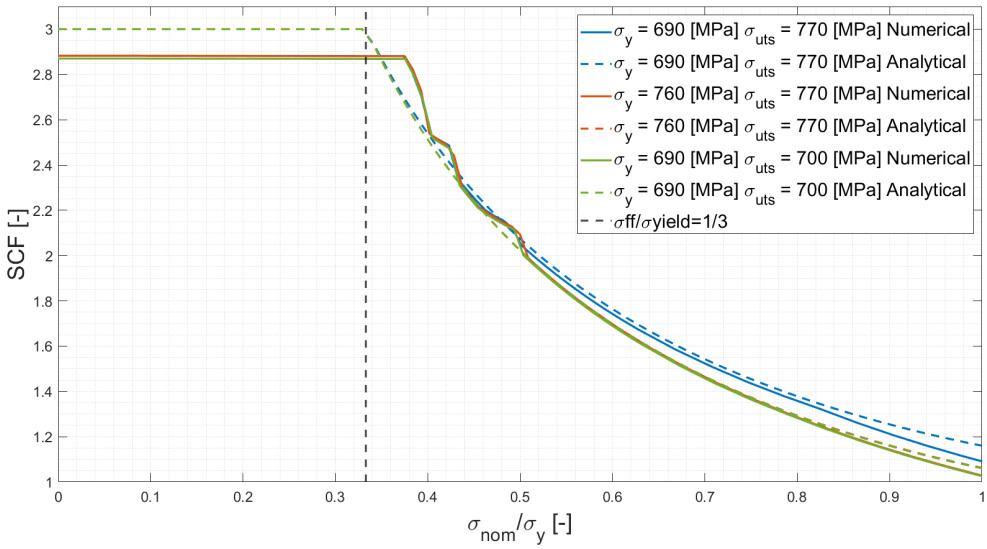

Figure B.1: SCF as a function of normalized nominal stress for different design cases at $\theta = \pi/2$ and r/a=1

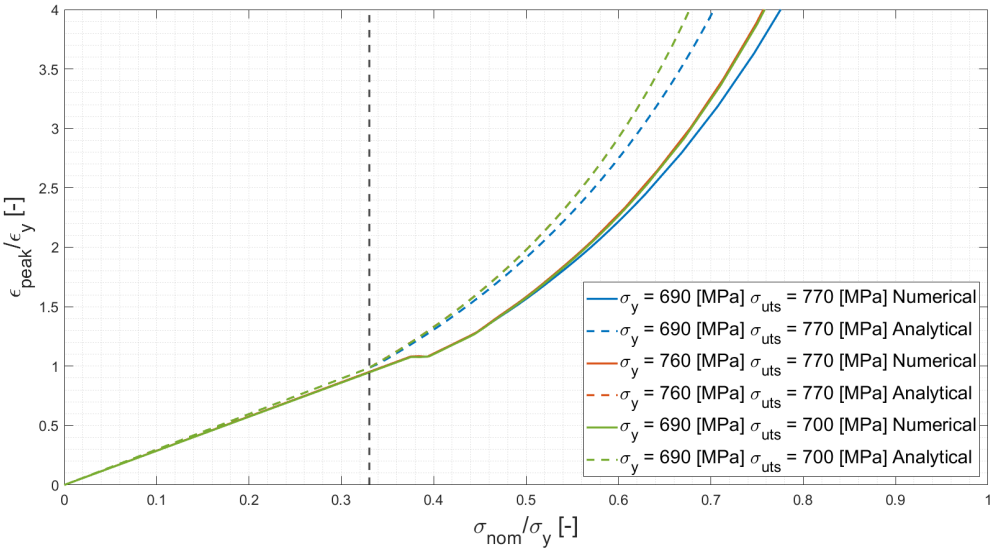

Figure B.2: Normalized local peak strain as a function of normalized nominal stress for different design cases at $\theta = \pi/2$ and r/a=1

Quantifying the results like in Section 7.7 for benchmark case I at $\frac{\sigma_{nom}}{\sigma_y} = 0.67$ gives Table B.2. This table shows the same local peak strain values after linear interpolation with corresponding allowable stresses. Using the material properties of case II results in a 1.90% lower allowable stress compared to the benchmark case. Using the material properties of case III results in an 1.66% decrease in allowable stress compared to the benchmark case.

Table B.2: Allowable stress for different design cases

	$\frac{\sigma_{nom}}{\sigma_y}$	ϵ_{peak}	Y/T [-]
Case I	0.67	2.798	0.896
Case II	0.6573	2.798	0.987
Case III	0.6589	2.798	0.986

Bibliography

[1] T.L. Anderson. *Fracture Mechanics; Fundamentals and applications*, volume 53. CRC Press, Boca Raton, 2013.

[2] A. C. Bannister, J. Ruiz Ocejo, and F. Gutierrez-Solana. Implications of the yield stress/tensile stress ratio to the SINTAP failure assessment diagrams for homogeneous materials. *Engineering Fracture Mechanics*, 67(6):547–562, 2000. ISSN 00137944.

[3] A.C. Bannister. Structural Integrity Assessment Procedures for European Industry Yield Stress / Tensile Stress Ratio : Results of Experimental Programme. Technical report, British Steel plc, Rotherham, 1999.

[4] A. Considère. Mémoire sur l'emploi du fer et de l'acier. *Annales des Ponts et Chaussées*, (9): 574–775, 1885.

[5] FEM(Fédération Européenne de la Manutention). *Rules of the design of hoisting appliances.* CEN, Brussels, 1998.

[6] D. S. Dugdale. Yielding of steel sheets containing slits. *Journal of the Mechanics and Physics of Solids*, 8(2):100–104, 1960. ISSN 00225096.

[7] CEN (European Committee for Standardization. *Cranes - General design - Part 3-1: Limit States and proof competence of steel structure.* CEN, Brussels, 2018.

[8] CEN (European Committee for Standardization. *Weldable structural steels for fixed offshore structures - technical delivery conditions.* CEN, Brussels, 2019.

[9] CEN (European Committee for Standardization. *Draft: Eurocode 3: Design of steel structures - Part 1-1: General rules and rules for buildings.* CEN, Brussels, 2020.

[10] L. Gardner and X. Yun. Description of stress-strain curves for cold-formed steels. *Construction and Building Materials*, 189:527–538, 2018. ISSN 0950-0618.

[11] R.C. Hibbeler. *Mechanics of Materials - SI Edition*. Pearson Education South Asia Pte Ltd, ninth edition, 2014.

[12] P. Hradil and A. Talja. True stress-strain relationship for finite element simulations of structural details under diffuse necking. *The 13th Nordic Steel Construction Conference (NSCC-2015)*, pages 229–230, 2015.

[13] P. Hradil and A. Talja. Ductility limits of high strength steels. *VTT Research Report*, 2016.

[14] Kirsch. Die Theorie der Elastizität und die Bedürfnisse der Festigkeitslehre. *Zeitschrift des Vereines deutscher Ingenieure*, (42):797–807, 1898.

[15] D. Kujawski. On energy interpretations of the Neuber's rule. *Theoretical and Applied Fracture Mechanics*, 73:91–96, 2014. ISSN 01678442.

[16] R. Kwesi Nutor. Using the Hollomon Model to Predict Strain-Hardening in Metals. *American Journal of Materials Synthesis and Processing*, 2(1):1–4, 2017. ISSN 2575-2154.

[17] B. N. Leis. Influence of Yield-to-Tensile Strength Ratio on Failure Assessment of Corroded Pipelines. *Journal of Pressure Vessel Technology*, 127(November):436–442, 2005.

[18] J. Lemaitre. *A course on damage mechanics*, volume 6. Springer, second edi edition, 1996. ISBN 9788578110796.

[19] DNV GL (Det Norske Veritas Germanischer Lloyd). *Standard: Offshore and platform lifting appliances.* DNV GL, Oslo, 2019.

[20] DNV GL (Det Norske Veritas Germanischer Lloyd). *Offshore standard: Metallic materials.* DNV GL, Oslo, 2020.

[21] DNV GL (Det Norske Veritas Germanischer Lloyd). *Rules for classification: Ships: Part 2 Materials and welding.* DNV GL, Oslo, 2020.

[22] B. McGinty. Fracture Mechanics, 2014. URL `https://www.fracturemechanics.org/hole.html`.

[23] K. Molski and G. Glinka. A method of elastic-plastic stress and strain calculation at a notch root. *Materials Science and Engineering*, 50(1):93–100, 1981. ISSN 00255416.

[24] 6892-1 NEN-EN-ISO. Metallic materials - Tensile testing - Part 1: Method of test at room: temperature (ISO 6892-1:2019,IDT). Technical report.

[25] H. Neuber. Theory of Stress Concentration for Shear-Strained Prismatical Bodies With Arbitrary Nonlinear Stress-Strain Law. *Journal of Applied Mechanics*, 28(4):544–550, 1961.

[26] H. Neuber. A physically nonlinear notch and crack model. *Journal of the Mechanics and Physics of Solids*, 16(4):289–294, 1968. ISSN 00225096.

[27] ABS (American Bureau of Shipping). *Guide for certification of lifting appliances.* ABS, Spring, 2020.

[28] R. Papirno. Plastic Stress-Strain History at Notch Roots in Tensile Strips under Monotonic Loading made on notched tensile strips under monotonically increasing loading. (October):446–452, 1971.

[29] W. D. Pilkey Pilkey, D. F, and Z. Bi. *Peterson's Stress Concentration Factors (4th Edition) - Charts*. John Wiley Sons., 2020. ISBN 9783319445557.

[30] W. M. Quach and J. F. Huang. Stress-Strain Models for Light Gauge Steels. *Procedia Engineering*, 14:288–296, 2011. ISSN 1877-7058.

[31] Kim J R Rasmussen. Full-range stress–strain curves for stainless steel alloys. *Journal of Constructional Steel Research*, 59(2003):47–61, 2006.

[32] Lloyd's Register. *Rules for the manufacture testing and certification of materials*. Lloyd's Register, London, 2020.

[33] Lloyd's Register. *Code for lifting appliances in a marine environment.* Lloyd's Register, London, 2020.

[34] K Sivakumaran. Role of Yield-To-Tensile Strength Ratio in the Design of. pages 63–76, 2010.

[35] M. Stofregen. Applicability of Design Rules for The Extra High Tensile Steel S1100Q. *MSc Thesis*, 2004, Delft University of Technology, The Netherlands.

[36] Z. E. Stowell. STRESS AND STRAIN CONCENTRATION AT A CIRCULAR. *National Advisory Committee For Aeronautics*, 1950.

[37] H. W. Swift. Plastic instability under plane stress. *Journal of the Mechanics and Physics of Solids*, 1:1–18, 1952.

[38] F. Tavakkoli and R. Ghajar. A new simple method for calculating notch root stress and strain of plane problems subjected to monotonic loading up to general yielding. *Journal of the Brazilian Society of Mechanical Sciences and Engineering*, 42(8):1–9, 2020. ISSN 18063691.

[39] Bureau Veritas. *Rules for the certification of lifting appliances onboard ships and offshore units.* Bureau Veritas, Neuilly sur Seine, 2020.

[40] Bureau Veritas. *Rules on materials and welding for the classification of marine units.* Bureau Veritas, Paris, 2020.

[41] Walters, C.L. Personal Correspondance, May 2021.

[42] W.J. Wong and C.L. Walters. Failure modes and rules related to the yield-to-tensile strength ratio in steel structures. *Proceedings of the International Conference on Offshore Mechanics and Arctic Engineering - OMAE*, 2021.

[43] R.N. Wright. *Wire Technology - Process Engineering and Metallurgy* . Elsevier Ltd., 2011.

[44] X. Yun and L. Gardner. Stress-strain curves for hot-rolled steels. *JCSR*, 133:36–46, 2017. ISSN 0143-974X.